The EMBO Journal vol.8. no.8 pp.2149 - 2170, 1989

NOBEL LECTURE

The photosynthetic reaction centre from the purple bacterium *Rhodopseudomonas viridis*

Johann Deisenhofer and Hartmut Michel[1]

Howard Hughes Medical Institute and Department of Biochemistry, University of Texas Southwestern Medical Center, 5323 Harry Hines Blvd, Dallas, TX 75235, USA and [1]Max-Planck-Institut für Biophysik, Heinrich-Hoffmann-Str. 7, D-6000 Frankfurt/M 71, FRG

In our lectures we first describe the history and methods of membrane protein crystallization, before we show how the structure of the photosynthetic reaction centre from the purple bacterium *Rhodopseudomonas viridis* was solved. Then the structure of this membrane protein complex is correlated with its function as a light-driven electron pump across the photosynthetic membrane. Finally we draw conclusions on the structure of the photosystem II reaction centre from plants and discuss the aspects of membrane protein structure. Sections 1 (crystallization), 4 (conclusions on the structure of photosystem II reaction centre and evolutionary aspects) and 5 (aspects of membrane protein structure) were presented and written by H.M., Sections 2 (determination of the structure) and 3 (structure and function) by J.D. We have arranged the paper in this way in order to facilitate continuous reading.

1. The crystallization

1.1. *The background*

As in many instances of new scientific developments and technical inventions an accidental observation caused the beginning of the experiments, which ultimately resulted in the elucidation of the three-dimensional structure of a photosynthetic reaction centre. This initiating observation in August 1978, was the formation of solid, glass-like aggregates when bacteriorhodopsin, de-lipidated according to Happe and Overath (1976) was stored in the freezer. These aggregates are shown in Figure 1A. From there on I was convinced that it should be possible not only to obtain these solid bodies but also to produce three-dimensional crystals. The availability of well-ordered three-dimensional crystals is the prerequisite for a high resolution X-ray crystallographic analysis, which—despite the progress made by Henderson and Unwin (1975) with electron microscopy and electron diffraction on bacteriorhodopsin—was and still is the only way to obtain a detailed structural knowledge of large biological macromolecules.

I was working at the university of Würzburg as a post-doc in the laboratory of D.Oesterhelt who, in collaboration with Walter Stoeckenius, had discovered bacteriorhodopsin (Oesterhelt and Stoeckenius, 1971) and was later the first to propose its function (Oesterhelt, 1972). My intention to try to produce well-ordered three-dimensional crystals of bacteriorhodopsin received his immediate support. It turned out that he had already tried to crystallize a modified form of bacteriorhodopsin in organic solvents.

Bacteriorhodopsin, the protein component of the so-called purple membrane resembles the visual pigment rhodopsin and acts as a light-energy converting system. It is part of a simple 'photosynthetic' system in halobacteria. It is an integral membrane protein, which forms two-dimensional crystals in the so-called purple membrane. At that time the general belief was that it was impossible to crystallize membrane proteins. With the exception of bacteriorhodopsin there was no information about the three-dimensional structure of membrane proteins, which might have helped to understand their various functions, e.g. as carriers, energy converters, receptors or channels.

The first attempts were to decrease the negative surface charge of the purple membrane by addition of long-chain amines and to add some Triton X-100, a detergent, in order to allow rearrangements of the bacteriorhodopsin molecules, which were partly solubilized by the detergent. This procedure might be a way to obtain the type-I crystals described below. Within 4 weeks the 'needles' presented in Figure 1B were obtained. Electronmicroscopic studies carried out in collaboration with Richard Henderson in Cambridge showed that the 'needles' were a new two-dimensionally crystalline membrane form of bacteriorhodopsin. In this new form the membranes are rolled up like tobacco leaves in a cigar (Michel *et al.*, 1980).

1.2. *A more systematic approach*

Based on the properties of membrane proteins, a new strategy was developed (Michel, 1983). Membrane proteins are embedded into the electrically insulating lipid bilayers. The difficulties in handling membrane proteins reside in the amphipathic nature of their surface. They possess a hydrophobic surface where, in the membrane, they are in contact with the alkane chains of the lipids, and they have a polar surface where they are in contact with the aqueous phases on both sides of the membrane and the polar head-groups of the lipids (see Figure 2). As a result membrane proteins are not soluble in aqueous buffers or in organic solvents of low dielectric constant. In order to solubilize membrane proteins one has to add detergents. Detergents are amphiphilic molecules which form micelles above a certain concentration, the so-called critical micellar concentration. The detergent micelles take up the membrane proteins and shield the hydrophobic surface parts of the membrane protein from contact with water. A schematic drawing of a biological membrane and its solubilization with detergents is shown in Figure 2. The membrane protein in the detergent micelle then has to be purified by various chromatographic procedures.

Once the protein has been isolated and is available in large quantities, one can try to crystallize it. For membrane proteins, which are merely anchored in the membrane, the most promising approach is to remove the membrane anchor by proteases or to use genetically modified material, where the part of the gene coding for the membrane anchor has

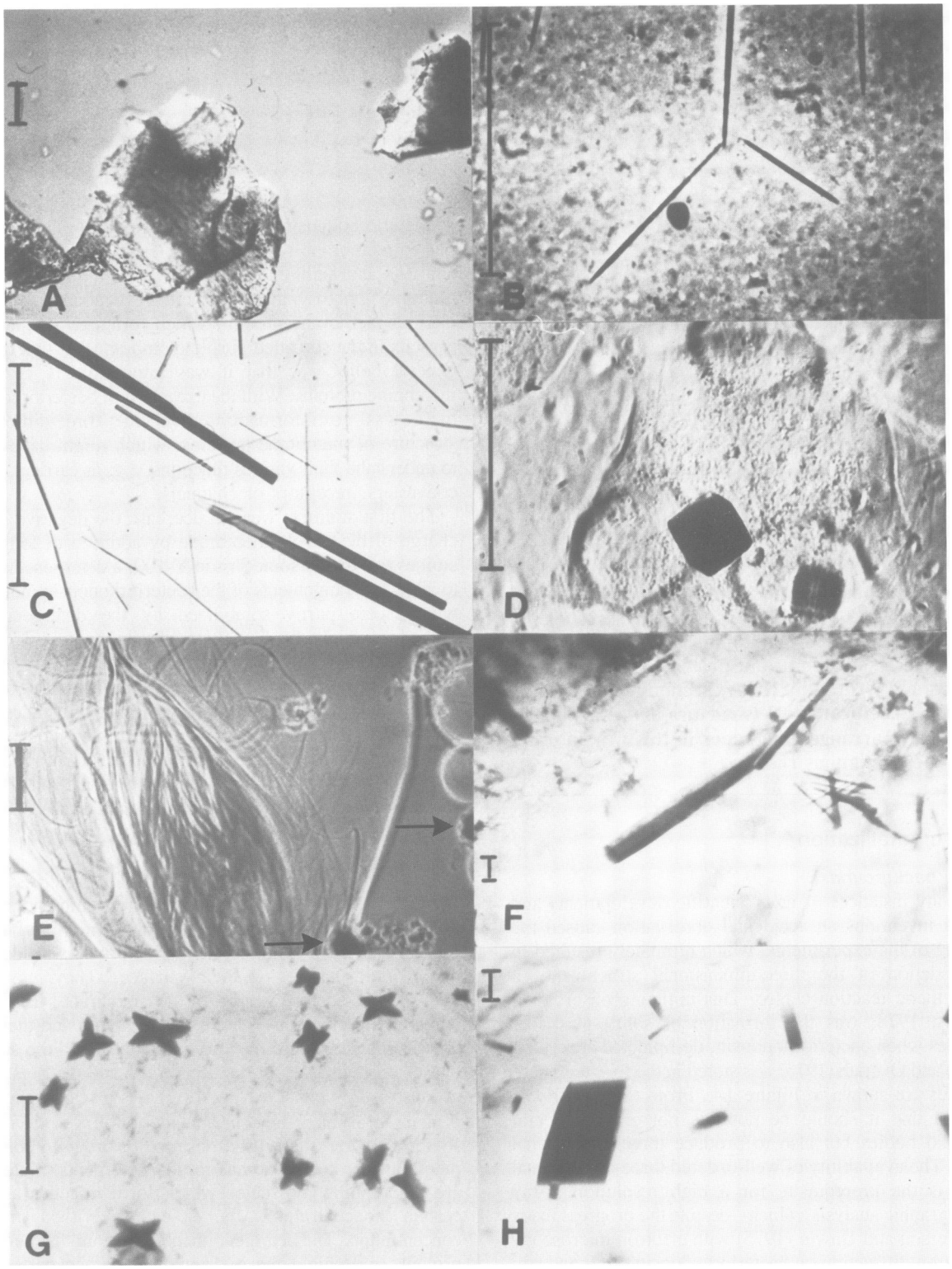

Fig. 1. Optical micrographs showing crystals and aggregates of bacteriorhodopsin and the photosynthetic RC from *R.viridis*: (**A**) aggregates of bacteriorhodopsin obtained after freezing of de-lipidated bacteriorhodopsin; (**B**) rolled up sheets of the two-dimensionally crystalline orthorhombic form of purple membrane (taken from Michel *et al.*, 1980); (**C**) needle-like crystals of bacteriorhodopsin obtained with sodium phosphate as precipitant; (**D**) cube-like crystals of bacteriorhodopsin obtained with ammonium sulphate as precipitant; (**E**) filamentous aggregates of bacteriorhodopsin and a few cubes (arrows) obtained with ammonium sulphate as precipitant (taken from Michel, 1982a); (**F**) hexagonal columns of bacteriorhodopsin obtained in the presence of 3% heptane-1,2,3-triol with ammonium sulphate as precipitant; (**G**) star-like RC crystals obtained within 2 days (starting conditions: 1 mg protein/ml, 3% heptane-1,2,3-triol, 1.5 M ammonium sulphate) by vapour diffusion against 3 M ammonium sulphate (taken from Michel, 1982b); (**H**) tetragonal crystals of the RC obtained within 3 weeks (starting conditions as in G) by vapour diffusion against 2.4 M ammonium sulphate (taken from Michel, 1982b). The bar indicates 0.1 mm in all photographs.

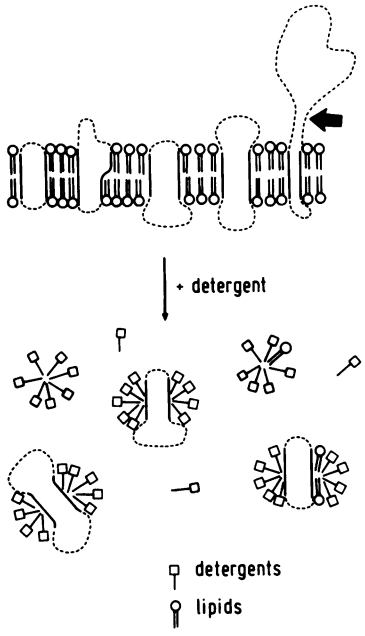

Fig. 2. Schematic drawing of a biological membrane (top) consisting of a lipid bilayer and membrane proteins embedded into it, and its solubilization by detergents (bottom). The polar part of the membrane protein surface is indicated by broken lines (modified after Michel, 1983).

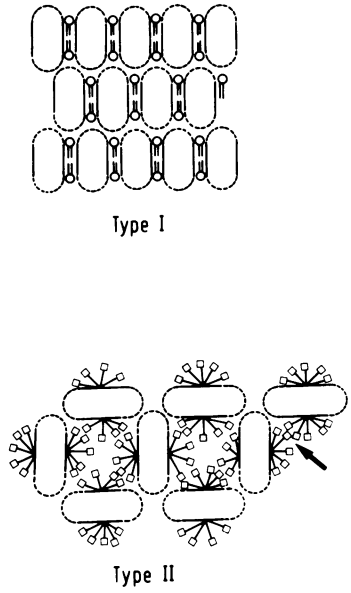

Fig. 3. The two basic types of membrane protein crystals. Type I: stacks of membranes containing two-dimensionally crystalline membrane proteins, which are then ordered in the third dimension. Type II: a membrane protein crystallized with detergents bound to its hydrophobic surface. The polar surface part of the membrane proteins is indicated by broken lines. The symbols for lipids and detergents are the same as in Figure 2 (taken from Michel, 1983).

been deleted. At present there are already four examples where the structures of the hydrophilic domains have been reported at high resolution: cytochrome b_5 (Mathews *et al.*, 1972), haemagglutinin (Wilson *et al.*, 1981) and neuraminidase (Varghese *et al.*, 1983) from influenza virus; and the human class I histocompatibility antigen. HLA-A2 (Bjorkmann *et al.*, 1987). For really integral membrane proteins two possibilities exist to arrange them in the form of true three-dimensional crystals.

(i) One could think of forming stacks of two-dimensional crystals of membrane proteins. In the third dimension the two-dimensional crystals must be ordered with respect to translation, rotation and up-and-down orientation during or after their formation. In most cases the lipids might still be present in the form of bilayers and compensate the hydrophobicity of the intramembranous protein surface. Hydrophobic and polar interactions would stabilize the crystals in the membrane planes, whereas polar interactions would dominate in the third dimension. In a reasonable crystallization procedure one would have to increase both types of interaction at the same time. This seems to be difficult to achieve.

(ii) The alternative is to crystallize the membrane proteins within the detergent micelles. The crystal lattice will be formed by the membrane proteins via polar interactions between polar surface parts. Figure 3 (bottom) shows one example of such a crystal. It is immediately clear that membrane proteins with large extramembranous domains should form this type of crystal much easier than those with small polar domains. The size of the detergent micelle plays a crucial role. A large detergent micelle might prevent the required close contact between the polar surface domains of the membrane proteins. One way to achieve a small detergent micelle is to use small linear detergents like octylglucopyranoside. However, a general experience of membrane biochemists is that membrane proteins in micelles formed by a detergent with a short alkyl chain are not very stable. An increase of the alkyl chain length by one methylene group frequently leads to an increase of the stability by a factor of two to three. One therefore has to find a compromise.

The advantage of the type II crystals is that basically the same procedures to induce supersaturation of the membrane protein solution can be used as for soluble proteins, namely vapour diffusion or dialysis with salts or polymers like polyethylene glycol as precipitating agents. A serious complication caused by the detergents is the frequent formation of a viscous detergent phase, which seems to consist of precipitated detergent micelles (see, for example, Zulauf *et al.*, 1985). Membrane proteins are enriched in the detergent phase, and frequently undergo denaturation. In several examples crystals which were already formed were redissolved.

Bacteriorhodopsin, solubilized in octylglucopyranoside, forms needle-like crystals (Figure 1C), when phosphate is used as precipitant (Figure 1C) and cubes, when ammonium sulphate (Figure 1D) is used (Michel and Oesterhelt, 1980). The cubes are not the most stable material, and a conversion into a hairy, thread-like material (Figure 1E) is found after several weeks (Michel, 1982a). In this hairy material bacteriorhodopsin probably forms membranes again.

OmpF-porin, an outer membrane protein from *Escherichia coli*, was also crystallized after solubilization in octyglucopyranoside by Garavito and Rosenbusch (1980). We received knowledge of this parallel development when

D.Oesterhelt and J.P.Rosenbusch met in China at the end of 1979.

1.3. *The improvement*

My feeling for the lack of the final success with bacteriorhodopsin was always that the detergent micelles were still too large. The use of even smaller detergents was impossible due to the insufficient stability of bacteriorhodopsin in detergents with a shorter alkyl chain or a smaller polar head group. One way out was to add small amphiphilic molecules (Michel, 1982a, 1983) for several reasons: (i) these molecules might displace detergent molecules which were too large to fit perfectly into the proteins crystal lattice in certain positions. (ii) The small amphiphilic molecules are too small to form micelles themselves, but they are incorporated into the detergent micelles. These mixed micelles are smaller than the pure detergent micelles and possess a different curvature of their surface. As a result the proteins could come closer together. (iii) Their polar head group is smaller than that of the detergent and less of the protein's polar suface would be covered by the polar part of the mixed small amphiphile/detergent micelle.

I had a look through the catalogues of the major chemical companies and ordered nearly everything which was polar at one end and hydrophobic at the other. In addition I synthesized ~20 amphiphilic compounds, mainly alkylpolyols and alkyl-*n*-oxides. These compounds were added during our attempts to crystallize bacteriorhodopsin. Several of the compounds had the effect that hexagonal columns (see Figure 1F) were obtained, whereas cubes (Figure 1D) had been obtained without the additives. The most effective compound was heptane-1,2,3-triol, but it had a slightly denaturing effect on bacteriorhodopsin. The diffraction quality of the bacteriorhodopsin crystals was improved: using synchrotron radiation H.Bartunik, D.Oesterhelt and myself found that they occasionally diffracted to 3 Å resolution, but only in one direction.

1.4. *The turn to classical photosynthesis*

Frustrated from the lack of the final breakthrough with bacteriorhodopsin, which is partly due to the absence of large extramembranous domains in this protein, I looked for more promising membrane proteins to be crystallized. My choices were the photosynthetic reaction centres (RCs) from the purple bacteria *Rhodospirillum rubrum* and *Rhodopseudomonas viridis* and the light-harvesting chlorophyll *a/b* protein from spinach. It was influenced by the fact that these proteins (or protein complexes) were said to be part of a two-dimensional crystalline array already in their native environment. As additional benefits they were available in large quantities, could easily be isolated, were coloured and denaturation of the proteins was indicated by colour changes.

I learned about the *R. viridis* system when E.Wehrli from the ETH Zürich presented the result of electron microscopical studies during a workshop at Burg Gemen, Germany, in June 1979 (Baumeister and Vogell, 1980). Initially, I received some isolated photosynthetic membranes from him in December 1980. At that time I had moved with D.Oesterhelt to the Max-Planck-Institut für Biochemie at Martinsried near Munich and I was just back from a stay at MRC in Cambridge where we had carried out X-ray diffraction experiments on the bacteriorhodopsin crystals. I isolated the RCs using hydroxyapatite chromatography

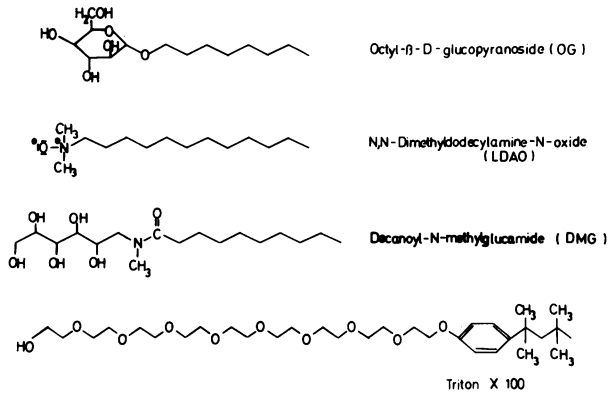

Fig. 4. Structural formulae of commonly used detergents: octylglucopyranoside, *N,N*-dimethyldodecylamine-*N*-oxide and decanoyl-*N*-methylglucamide are promising for membrane protein crystallization, whereas Triton X-100 is not.

according to a published procedure (Clayton and Clayton, 1978) and tried to crystallize it, without success. I developed a new isolation procedure using only molecular sieve chromatography, and tried it again with immediate success (Michel, 1982b). The conditions were nearly identical to those found to be optimal for bacteriorhodopsin. The exception was that I could use *N,N*-dimethyldodecylamine-*N*-oxide as detergent instead of octylglucopyranoside (see Figure 4). In the presence of 3% heptane-1,2,3-triol (high melting point isomer) and 1.5–1.8 M ammonium sulphate, star-like crystals are obtained upon vapour diffusion against 2.5–3 M ammonium sulphate in 2 days, more regular tetragonal columns with a length of up to 2 mm upon vapour diffusion against 2.2–2.4 M ammonium sulphate in 2–3 weeks (see Figure 1G and H). The much smaller polar head group of *N,N*-dimethyldodecylamine-*N*-oxide is certainly of importance. Unfortunately, this detergent denatures bacteriorhodopsin. D.Oesterhelt generously considered the RC as my project.

The crystals turned out to be of excellent quality from the beginning. After a scaling up of the isolation procedure, a continuous supply of crystals was guaranteed. I could then start collecting the X-ray data with the initial help of W.Bode and R.Huber. Figure 5 shows a rotation photograph similar to that used for data collection.

2. Determination of the structure

In spring 1982 I (J.D.) joined H.M. in order to determine the three-dimensional structure of the RC. The tetragonal crystals have unit cell dimensions of $a = b = 223.5$ Å, $c = 113.6$ Å, and the symmetry of space group $P4_32_12$ (Michel, 1982b; Deisenhofer *et al.*, 1984). As it turned out, there is one RC with a mol. wt of 145 000 daltons in the asymmetric unit.

2.1. *Collection of X-ray reflection intensity data*

For data collection we used the rotation method with a rotating anode X-ray generator as the source, and photographic film as the detector (Deisenhofer *et al.*, 1984). The large unit cell of the RC crystals, in combination with the resolution limit of the diffraction pattern at 2.9 Å limited the rotation interval per film exposure to 0.5°, so that more than two thirds of the reflections on any given film were

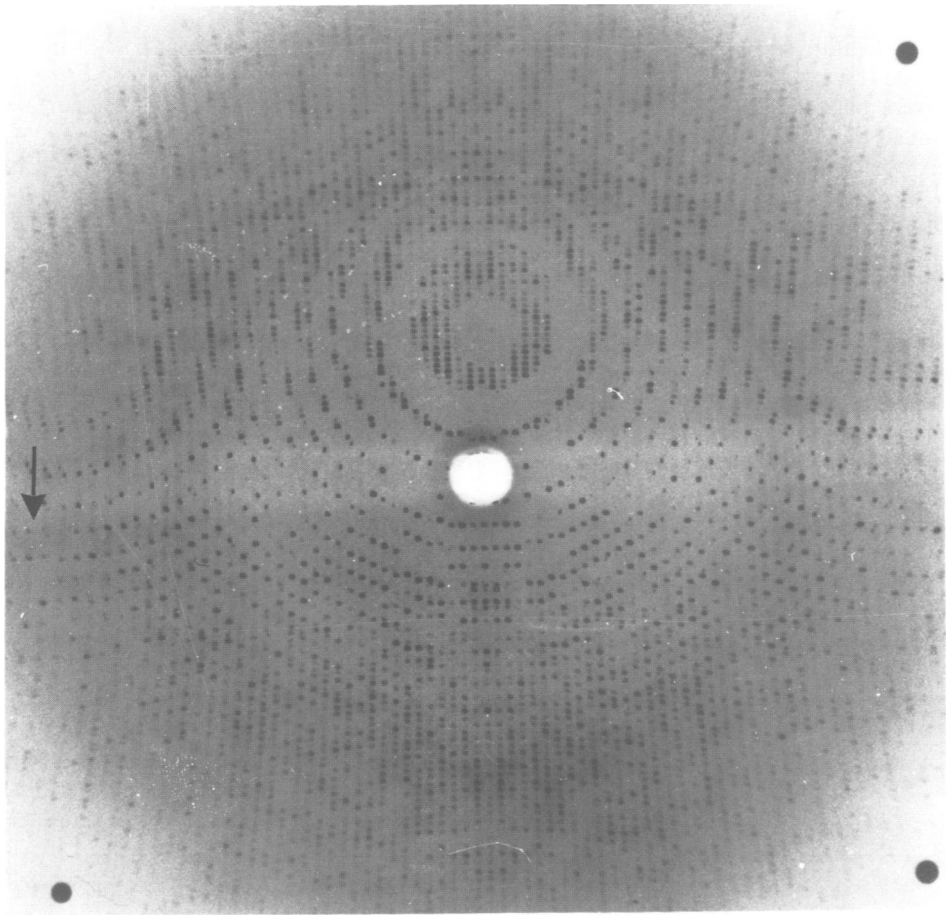

Fig. 5. X-ray diffraction pattern of a single RC crystal (1° rotation). Exposure time: 20 h, Cu-K_α-radiation, crystal-to-film distance: 100 mm. The arrow indicates 3.0 Å resolution (taken from Michel, 1982b).

partially recorded. However, the long lifetime of the crystals in the X-ray beam at ~0°C, and their positional stability allowed the adding up of partially recorded reflections from successive exposures, so that their treatment did not present a serious problem. Nevertheless, it took ~3–4 months to collect a complete data set. Data collection for the heavy atom derivatives was speeded up by choosing a rotation interval of 0.6° per exposures. A later re-collection of the native data set at the HASYLAB facilities of DESY in Hamburg was carried out at 2.3 Å resolution in rotation intervals of 0.4° by Irmgard Sinnig, Gerhard Schertler and H.M. The most tedious and time-consuming task in this type of data collection was the processing of films. Kunio Miki and later Otto Epp provided most valuable help during that period of the work. We used the computer programs FILME (Schwager *et al.*, 1975; Jones *et al.*, 1977) and OSC (Rossmann, 1979; Schmid *et al.*, 1981) for film evaluation, and PROTEIN (principal author W.Steigemann) for scaling and merging data.

2.2. *Solution of the phase problem*

To solve the phase problem for the RC crystal structure we used the method of isomorphous replacement with heavy atom compounds. The experimental part was performed by H.M., the film evaluation and data analysis by myself with support from Kunio Miki and Otto Epp. In order to find the heavy atom derivatives, crystals were soaked for 3 days in 1 mM solutions of the respective heavy atom compounds in a soak buffer similar to the mother liquor. A number of compounds like K_2PtBr_4, $K_2Pt(CN)_4$, $KHg(CN)_2$, K_2HgI_4 and $EuCl_3$ could not be used since they induced the phase separation of the soak buffer into the viscous detergent phase and the aqueous phase. At the beginning large heavy atom compounds like $(C_6H_5)_3PbNO_3$ or C_6H_5HgCl completely abolished the diffraction, whereas the smaller homologues $(CH_3)_3PbCl$ or C_2H_5HgCl decreased the diffraction to ~6 Å resolution. However, after additional purification of the RCs prior to crystallization, the diffraction quality of the crystals was unchanged by the small heavy atom compounds. One compound ($KAuCl_4$) caused a shrinkage of the *c*-axis. Rotation photographs (1°) showing a large part of the 1,*k*,*l* lattice plane were taken and inspected visually for changes in the diffraction pattern. For promising candidates, ~50% complete data sets were collected and evaluated.

On average, each heavy atom derivative had nine heavy atom binding sites (Deisenhofer *et al.*, 1984). The major binding sites were found with the automatic search procedure in the PROTEIN program package. Using five different heavy atom derivatives, we could calculate phases to 3.0 Å resolution, and an electron density map (Deisenhofer *et al.*, 1984). Phases and map were further improved by solvent flattening (Wang, 1985).

2.3. *Model building*

Map interpretation and model building was carried out in three stages. (i) The prosthetic groups in the RC were

identified. We found four haem groups, four bacteriochlorophyll *b* (BChl-b) two bacteriopheophytin *b* (BPL-b) and one quinone (Deisenhofer *et al.*, 1984). (ii) The polypeptide chains were built with polyalanine sequence, except in the N-terminal regions of the subunits L and M and cytochrome where partial amino acid sequences were known (Michel *et al.*, 1983), and could be used to distinguish between the subunits. At that stage, some use was made of the local symmetry of the subunits L and M. (iii) As the gene sequences of the RC subunits were determined (Michel *et al.*, 1985; Michel *et al.*, 1986a; Weyer *et al.*, 1987a), the model of the protein subunits was completed. The sequence information led to an overall verification but also to a number of minor corrections of the polypeptide backbone model, since in the previous model-building stage the electron density was not always clear enough to allow determination of the correct number of amino acids.

Our tools for model building were interactive graphics display systems: a black and white Vector General 3400 system and later a colour Evans & Sutherland PS 300. On both systems we used Alwyn Jones' programme package FRODO (Jones, 1978). The model library of this package was extended to include BChl-b, BPh-b, menaquinone-7 and ubiquinone-1. Frequent use was made of the real-space-refinement facility in FRODO which allowed long stretches of helical structure to be correctly placed into the electron density.

2.4. *Model refinement*

The RC model, with about half of the side chains of the cytochrome subunit still missing, already had the rather low crystallographic R value of 0.359 at 2.9 Å resolution ($R = \Sigma(||F_{obs}| - |F_{calc}||)/\Sigma|F_{obs}|$; where F_{obs} and F_{calc} are observed and calculated structure factors respectively). Crystallographic refinement of the model was started at 2.9 Å resolution and continued at 2.3 Å resolution. The programme packages used for refinement were PROTEIN, EREF (Jack and Levitt, 1978; Deisenhofer *et al.*, 1985b), TNT (Tronrud *et al.*, 1987) and again FRODO.

As a result of the refinement of R value was brought down to 0.193 for 95 762 unique reflections at 2.3 Å resolution, the refined model consisting of 10 288 non-hydrogen atoms. Errors in the initial model, e.g. peptide groups and side chains with wrong orientations, were removed. New features were added to the model: a partially order carotenoid molecule, a ubiquinone in the partially occupied Q_B binding pocket, a complete detergent molecule (LDAO), a candidate for a partially ordered LDAO or similar molecule, seven candidates for negative ions and 201 ordered water molecules. The upper limit of the mean coordinate error was estimated (Luzzati, 1952) to be 0.26 Å. The detailed description of refinement and refined model of the photosynthetic RC from *R. viridis* will be given elsewhere (J.Deisenhofer, O.Epp, I.Sinning and H.Michel to be published).

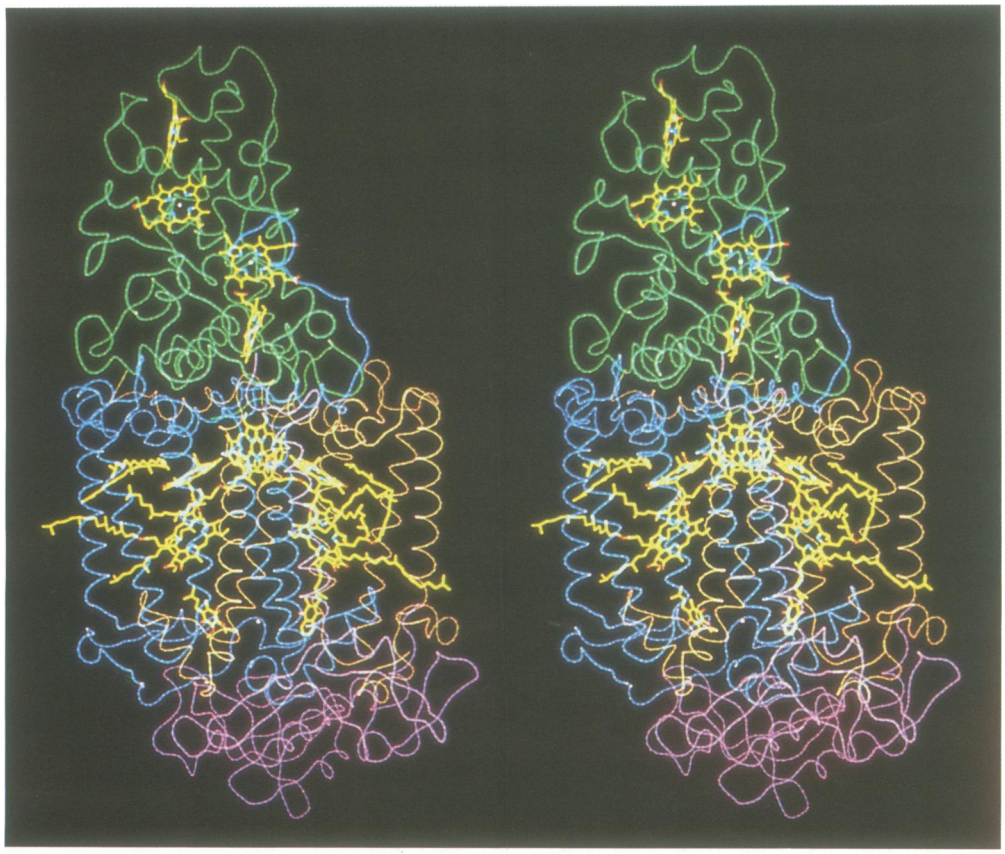

Fig. 6. Stereo pair showing an overall view of the RC structure. Protein chains are represented as smoothed backbone drawings: green, cytochrome; blue, M-subunit; brown, L-subunit; purple, H-subunit. Cofactors are drawn in bright atom-colours: yellow, carbons; blue, nitrogens; red, oxygens; green, magnesium. Smoothed backbone representations of polypeptide chains were produced following an idea of Richard J.Feldman, with help from Marius G.Clore.

3. Structure and function

3.1. *Structure overview*

An overall view of the structure of the photosynthetic RC from *R. viridis* is shown in Figure 6. It is a complex of four protein subunits and of 14 cofactors. The protein subunits are called H (heavy), M (medium), L (light) and cytochrome; the names H, M and L were chosen according to the apparent mol. wts of the subunits, as determined by electrophoresis. The core of the complex is formed by the subunits L and M, and their associated cofactors: four BChl-b, two BPh-b, one non-haem iron, two quinones and one carotenoid. Structural properties, e.g. the hydrophobic nature of the protein surface, and functional considerations strongly indicate that the subunits L and M span the bacterial membrane. This aspect of the structure will be discussed in detail below. Each of the subunits L and M contains five membrane-spanning polypeptide segments, folded into long helices. The polypeptide segments connecting the transmembrane helices form flat surfaces parallel to the membrane surfaces.

The H-subunit contributes another membrane-spanning helix with its N-terminus near the periplasmic membrane surface. The C-terminal half of the H-subunit forms a globular domain that is bound to the L−M complex near the cytoplasmic membrane surface. On the opposite side of the membrane the cytochrome subunit with its four covalently bound haem groups is attached to the L−M complex. Both the cytochrome subunit and the globular domain of the H-subunit have surface properties typical of water-soluble proteins.

The total length of the RC, from the tip of the cytochrome to the H-subunit is ~130 Å. The core has an elliptical cross-section with axes of 70 and 30 Å.

The photosynthetic RCs from purple bacteria are the best characterized among all photosynthetic organisms (for reviews see (Feher and Okamura, 1978; Okamura *et al.*, 1982). All of them contain the three subunits H, M and L; some bacteria lack the tightly bound cytochrome subunit. An example of a RC without a bound cytochrome subunit is that from *Rhodobacter sphaeroides* which was crystallized (Allen and Feher, 1984; Chang *et al.*, 1985); its structure has been shown to be very similar to the RC from *R. viridis* (Allen *et al.*, 1986; Chang *et al.*, 1986).

3.2. *Subunit structure*

Schematic drawings of the polypeptide chain folding of the four RC subunits are shown in Figure 7. As mentioned above, major elements of secondary structure in the subunits L and M are the five membrane-spanning helices. A comparison of the polypeptide chain folding in both subunits shows a high degree of similarity. Structurally similar segments include the transmembrane helices and a large fraction of the connections. In total, 216 α-carbons from the M-subunit can be superimposed onto corresponding α-carbons of the L-subunit with an r.m.s. deviation of only 1.22 Å. The superposition of the subunits is carried out by a rotation of ~180° around an axis running perpendicular to the membrane surface; we call this axis the central local symmetry axis. Table I lists the helices in both subunits, while Table II lists the structurally similar regions in both subunits. Besides the transmembrane helices, called LA, LB, LC, LD and LE, and MA, MB, MC, MD and ME, with lengths between 21 and 28 residues, there are shorter helices in the connecting segments, notably helix de (between transmembrane helices D and E), and helix cd. Subunit M (323 residues) is 50 residues longer than L (273 residues). The insertions in M, with respect to L, are located near the N-terminus (20 residues), in the connection between the helices MA and MB (seven residues), in the connection between MD and ME (seven residues), and at the C-terminus (16 residues). The insertions at the N- and C-termini make the M-subunit dominate the contacts with the peripheral subunits. The insertion between MD and ME, containing another small helix (see Table I) is of importance for the different conformations of the quinone-binding sites in L and M, and for binding of the non-haem iron (see below).

The H-subunit with 258 residues can be divided into three structural regions with different characteristics (see Figure 7). The N-terminal segment, beginning with formyl-methionine (Michel *et al.*, 1985), contains the only transmembrane helix of subunit H; it includes 24 residues from H12 to H35. Near the end of the transmembrane helix the sequence shows seven consecutive charged residues (H33−H39). Residues H47−H53 are disordered in the crystal, so that no significant electron density can be found for them.

Following the disordered region the H-chain forms an extended structure along the surface of the L−M complex, apparently deriving structural stability from that contact. The surface region contains a short helix and two two-stranded antiparallel β-sheets.

The third structural segment of the H-subunit, starting at about H105 forms a globular domain. This domain contains an extended system of antiparallel and parallel β-sheets between residues H134 and H203, and an α-helix (residues H232−H248). The β-sheet region, the only larger one in the whole RC, forms a pocket with highly hydrophobic interior walls. This structural property is reminiscent of transport proteins, e.g. retinol-binding protein (Newcomer *et al.*, 1984), bilin-binding protein (Huber *et al.*, 1987), and others; however, the strand topology is different. So far, no evidence for a ligand has been found.

With 336 residues (Weyer *et al.*, 1987c) the cytochrome is the largest subunit in the RC complex. Its last four residues, C333−C336, are disordered. Also disordered is the lipid molecule bound to the N-terminal cysteine residue (Weyer *et al.*, 1987a,b). The complicated structure of the cytochrome can be summarized as follows. The structure consists of an N-terminal segment, two pairs of haem-binding segments, and a segment connecting the two pairs. Each haem-binding segment consists of a helix with an average length of 17 residues, followed by a turn and the Cys-X-Y-Cys-His sequence typical of *c*-type cytochromes. The haems are connected to the cysteine residues via thioether linkages. This arrangement leads to the haem planes being parallel to the helix axes. The sixth ligands to the haem irons are in three of the four cases of methionine residues within the helices. The iron of haem 4 has histidine C124, located in a different part of the structure, as a sixth ligand. The two pairs of haem-binding segments, containing haem, 1 and 2, and 3 and 4 respectively, are related by a local 2-fold symmetry. From each pair 65 residues obey this local symmetry with an r.m.s. deviation between corresponding

α-carbon atoms of 0.93 Å. The local symmetry of the cytochrome is not related to the central local symmetry.

3.3. *Arrangement of cofactors*

Figure 8 shows the arrangement of the 14 cofactors associated with the RC protein subunits. The four haem groups of the cytochrome, numbered according to the order of attachment to the protein, form a linear chain that points to a closely associated pair of BChl-bs. This pair, the so-called 'special pair' is the origin of two branches of cofactors, each consisting of another BChl-b (the 'accessory' BChl-b), a BPh-6 and a quinone. The non-haem iron sits between the quinones. The tetrapyrrole rings of BChl-bs, BPh-bs and quinones follow approximately the same local symmetry that is displayed by the L- and M-chains. The branches of cofactors from the special pair to the BPh-bs can be clearly associated with subunits L or M, so that we speak of an L-branch and an M-branch.

This is the basis for our nomenclature: BChl-bs and BPh-bs are called BC_{XY} and BP_X respectively, where X denotes the branch (L or M), and Y is P for 'special pair' or A for 'accessory'. At the level of the quinones the situation is more complicated because the subunits interpenetrate here, and the quinone at the end of the L-branch is actually bound in a pocket of the M-subunit and *vice versa*. Therefore, we prefer the nomenclature Q_A and Q_B with Q_A at the end of the L-branch. Q_A is menaquinone-9, and Q_B is ubiquinone-9 (Gast *et al.*, 1985). The local symmetry is violated by the phytyl chains of BChl-bs and BPh-bs, by the different chemical nature and different occupancy of the quinones, and by the presence of a carotenoid molecule near the accessory BChl-b of the M-branch.

3.4. *Functional overview*

The current understanding of the function of the RC was developed by combining structural information with information from other experimental techniques, notably spectroscopy, as described in recent reviews (Parson and Ke, 1982; Kirmaier and Holten, 1987; Parson, 1987). Figure 9 shows a schematic view of the RC with its cofactors in

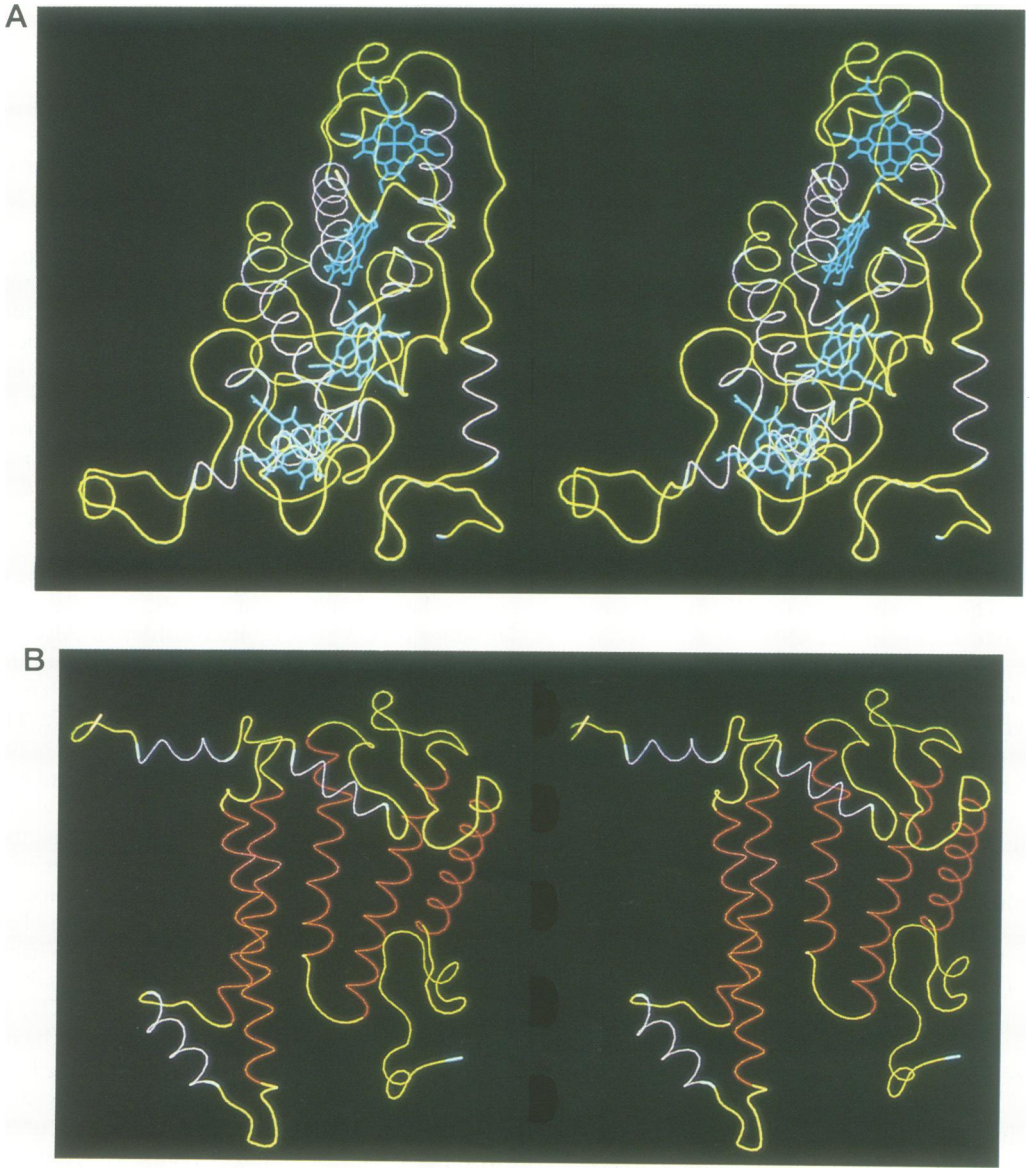

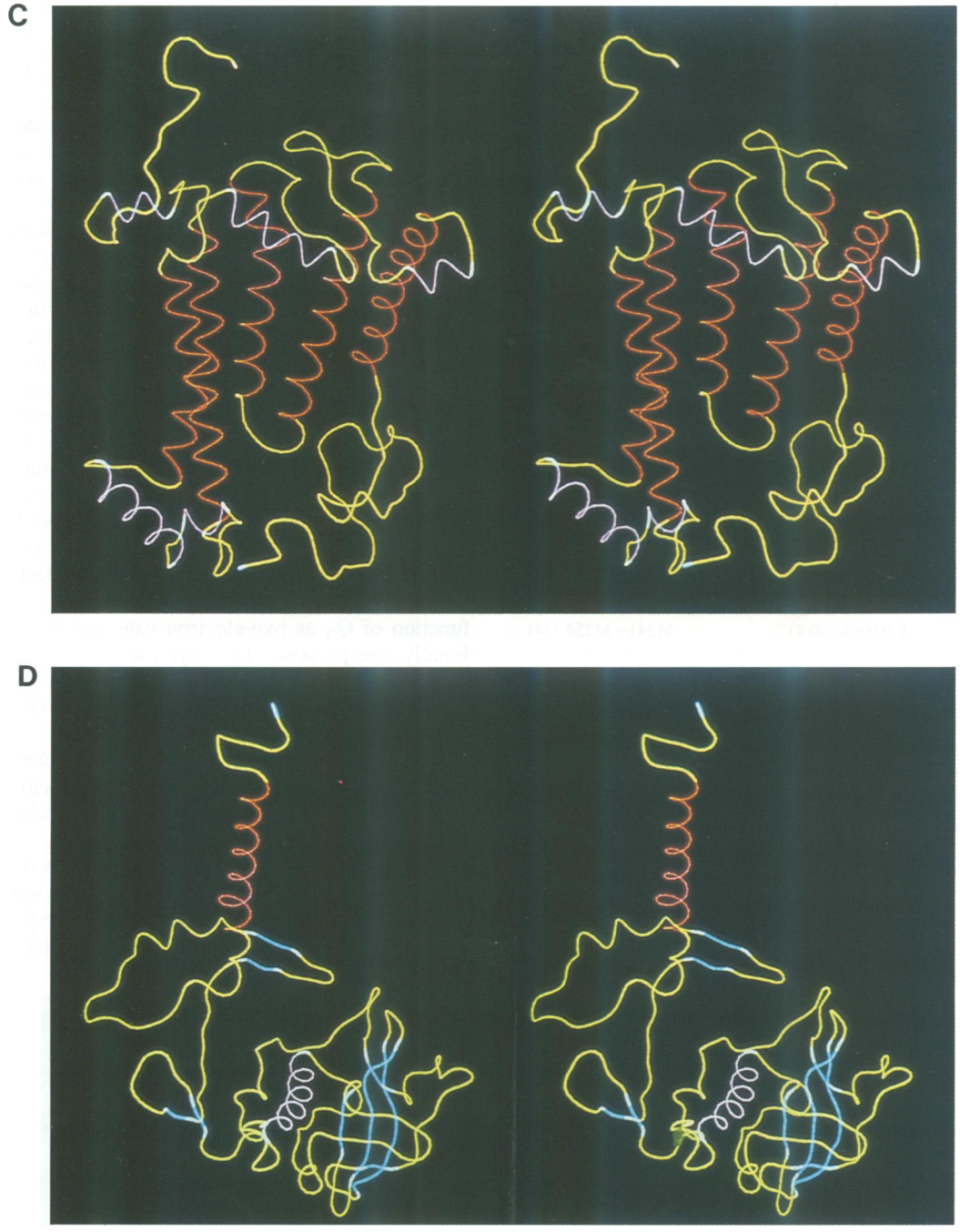

Fig. 7. Stereo pairs showing smoothed backbone representations of the protein subunits. Secondary structure is indicated by colours: yellow, no apparent secondary structure; red, transmembrane helices; purple, other helices; blue, antiparallel β-sheets. (**A**) Cytochrome (with the four haem groups); (**B**) L-subunit; (**C**) M-subunit; (**D**) H-subunit. N-termini are marked blue, C-termini are marked red.

the bacterial membrane. The special pair, P, is the starting point for a light-driven electron transfer reaction across the membrane. Absorption of a photon, or energy transfer from light-harvesting complexes in the membrane puts P into an excited state, P*. From P* an electron is transferred to the BPh-b on the L-branch, BP_L, with a time constant of 2.8 ps (Breton *et al.*, 1986; Fleming *et al.*, 1988). The distinction between the two BPh-bs was possible because they absorb at slightly different wavelengths and, with the knowledge of the crystal structure, linear dichroism absorption experiments could distinguish between the two chromophores (Zinth *et al.*, 1983, 1985; Knapp *et al.*, 1985).

From BP_L the electron is transferred to Q_A with a time constant of $\sim$200 ps. At this point the electron has crossed most of the membrane. Both these electron-transfer steps function at very low temperatures ($\sim$1°K) with time constants even shorter than at room temperature (Kirmaier *et al.*, 1985a,b). From Q_A the electron moves on to Q_B with $\sim$100 μs. The non-haem iron does not seem to play an essential role in this step (Debus *et al.*, 1986).

Q_B can pick up two electrons and, subsequently, two protons (Dracheva *et al.*, 1988). In the Q_BH_2 state it dissociates from the RC, and the Q_B site is re-filled from a pool of quinones dissolved in the membrane. Electrons and protons on Q_BH_2 are transferred back through the membrane by the cytochrome b/c_1 complex. The electrons are shuttled via a soluble cytochrome c_2 to the RC's cytochrome from which P^+ had been reduced with a time constant of ~270 μs. This time constant increases with decreasing temperature down to ~100°K, and remains constant for lower temperatures. The whole process can be described as a light-driven cyclic electron flow, the net effect of which is the generation of a proton gradient across the membrane that is used to synthesize adenosine triphosphate, as described by P.Mitchell's chemiosmotic theory.

Complete understanding of the RC's function still meets with a number of problems: the nature of electron transfer along the stages described above, and its speed and temperature dependence have not been explained theoretically yet. The first step, with the question of the role of the bridging BC_{LA}, is a matter of fascinating debate.

One of the major surprises from the structural work was the symmetry of the core structure, raising the question of the factors leading to the use of only the L-branch of cofactors and of the significance of the apparently unused branch. Further open questions relate to electron transfer between Q_A and Q_B, the role of the non-haem iron and the function of Q_B as two-electron gate and proton acceptor. Finally, the purpose of the cytochrome, as well as details of electron transfer from the soluble cytochrome and among the four haems, is not as yet completely explained.

Table I. Helical segments in subunits L and M

Helix	Segment (length)	
	Subunit L	Subunit M
Transmembrane		
A	L33–L53 (21)	M52–M76 (25)
B	L84–L111 (28)	M111–M137 (27)
C	L116–L139 (24)	M143–M166 (24)
D	L171–L198 (28)	M198–M223 (26)
E	L226–L249 (24)	M260–M284 (25)
Periplasmic		
	–	M81–M87 (7)
cd	L152–L162 (11)	M179–M190 (12)
ect	L259–L267 (9)	M292–M298 (7)
Cytoplasmic		
	–	M232–M237 (6)
de	L209–L220 (12)	M241–M254 (14)

Table II. Regions with similar polypeptide chain folding in subunits L and M

Subunit M		Subunit L	Length
M49–76	→	L29–56	28
M88–96	→	L61–69	9
M100–224	→	L73–197	125
M243–290	→	L209–256	48
M291–296	→	L258–263	6

3.5. *Structural details in relation to function*

Here I describe the arrangement of the cofactors, and their environment in some detail. Observations relating to open functional questions are emphasized.

Figure 10 shows the BChl-b ring systems of the special pair, the primary electron donor of the photosynthetic light reaction. On the basis of spin-resonance experiments the existence of a special pair had been postulated a long time

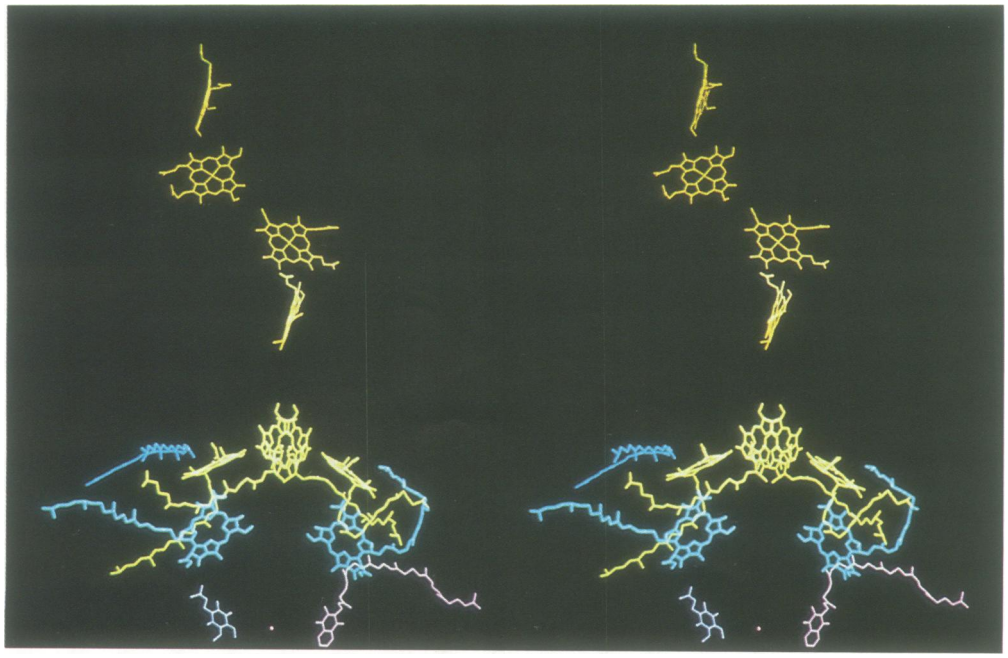

Fig. 8. Stereo view of the cofactors. Brown, haem groups; yellow, bacteriochlorophyll-bs; light blue, bacteriophaeophytin-bs; blue, carotenoid (dihydro-neurosporene; I.Sining and H.Michel, unpublished results); purple, quinones (right, Q_A, left, Q_B); red dot, non-haem iron.

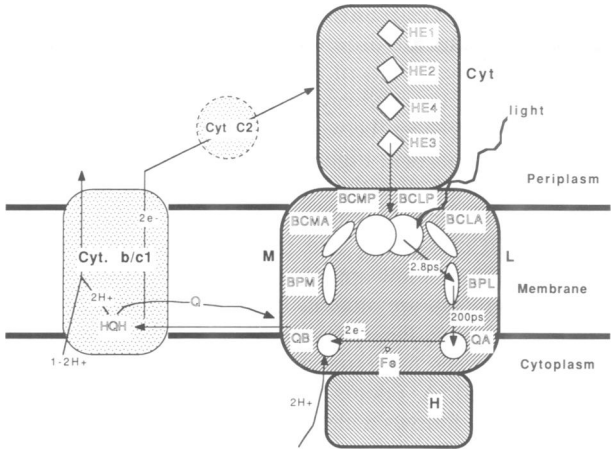

Fig. 9. Schematic view of the RC, showing the light-driven cyclic electron flow.

ago (Norris *et al.*, 1971). The two molecules overlap with their pyrrole rings I in such a way that, when looking in a direction perpendicular to the ring planes, the atoms of these rings eclipse each other. The orientation of the rings leads to a close proximity between the ring I acetyl groups, and the Mg^{2+} ions; however, the acetyl groups do not act as ligands to the Mg^{2+}. The pyrrole rings I of both BChl-bs are nearly parallel and ~3.2 Å apart. Both tetrapyrrole rings, however, are non-planar; planes through the pyrrole nitrogens of each BChl-b form an angle of 11.3°.

The special pair BChl-bs are arranged with a nearly perfect 2-fold symmetry. This is illustrated also in Figure 11 which shows a view along the 2-fold axis (Deisenhofer and Michel, 1988). The BChl-b rings of the special pair are nearly parallel to the symmetry axis. Further objects, shown in Figure 11, that obey the central local 2-fold symmetry are the histidine residues (L173 and M200), acting as ligands to the special pair Mg^{2+} ions, the rings of the accessory BChl-bs, the

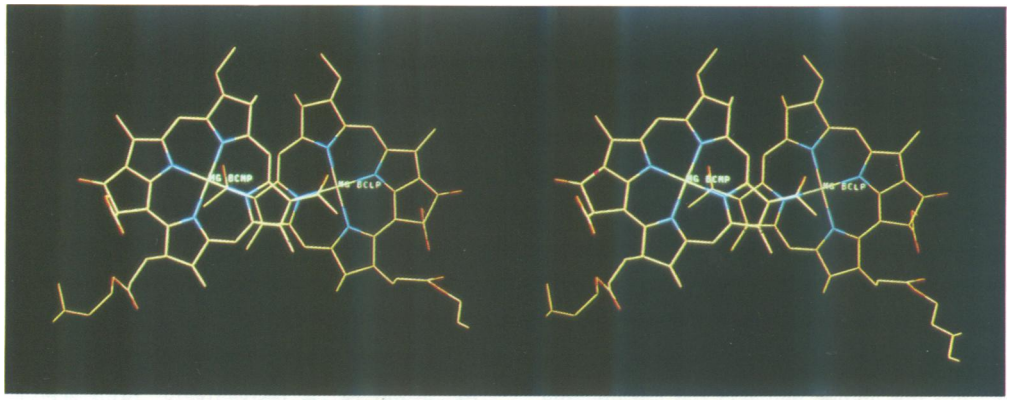

Fig. 10. Stereo view of the special pair in atom colours: yellow, carbons; blue, nitrogens; red, oxygens; green, magnesium.

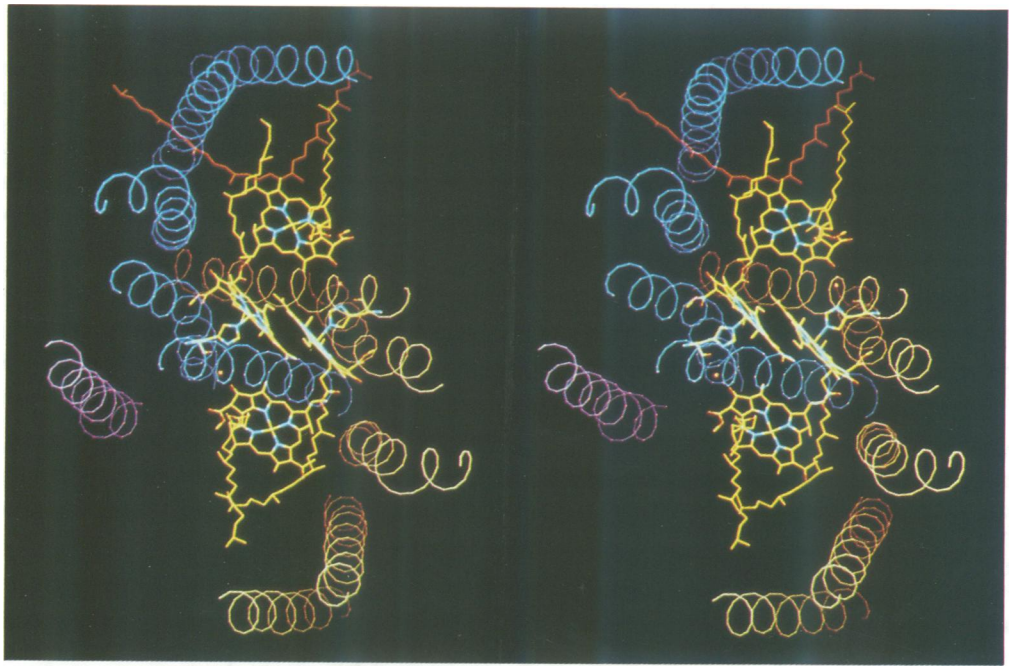

Fig. 11. Stereo pair: view along the central local 2-fold axis showing in atom colours: special pair with histidine ligands, accessory bacteriochlorophyll-bs (BC_{LA} bottom, BC_{MA} top), two waters; the transmembrane helices of subunits L (brown), M (blue) and H (purple) are shown in smoothed backbone representation.

water molecules H-bonded between histidine nitrogens and ring V carbonyl groups of the accessory BChl-bs, and the transmembrane helices of subunits L and M. The carotenoid molecule in contact with the accessory BChl-b, BC_{MA}, the side chains of the accessory BChl-bs, and the transmembrane helix of the H-subunit are examples of structural elements that break the 2-fold symmetry. A more subtle deviation from symmetry is the different degrees of non-planarity of the two BChl-b ring systems of the special pair. The BC_{MP} ring is considerably more deformed than that of BC_{LP}. This can cause an unequal charge distribution between the two components of the special pair, which in turn can be part of the reason for unidirectional electron transfer (Michel-Beyerle *et al.*, 1988).

Even though the tetrapyrrole rings of the BChl-bs and BPh-bs of the L- and M-branches can be rotated on top of each other using a single transformation with the reasonably low r.m.s. deviation of 0.38 Å between the positions of equivalent atoms, a closer inspection shows considerable differences between the local symmetry operations of special pair, accessory BChl-bs and BPh-bs. Optimum superposition of the tetrapyrrole rings of the special pair alone is achieved by a rotation of 179.7°, for the accessory BChl-bs by a rotation of −175.8° and for the BPh-bs by a rotation of −173.2°. This deviation from 2-fold symmetry is illustated in Figure 12, where the cofactors of the M-branch were rotated using the transformation that optimally superimposes the special pair tetrapyrrole rings. It is clear that, due to the imperfect symmetry, interatomic distances and interplanar angles are different in both branches. For example, the closest distance of atoms involved in double bonds in the special pair and in BP_L is shorter by 0.7 Å than the corresponding distance between the special pair and BP_M. Another example are the angles between the tetrapyrrole rings of the special pair, and those of the accessory BChl-bs: the angles of BP_L are ~6° smaller than for BP_M. These structural differences lead to differences in overlap of electronic orbitals, and are expected to lead to different electron transfer properties in both branches. This may be another contribution to the undirectional charge separation in the RC.

Yet another observation that may relate to the different electronic properties of the L- and M-branches is the different degree of structural order. The amount of disordered structure, measured by the number of atoms without significant electron density, is larger in the constituents of the M-branch than in those of the L-branch. Both phytyl side chains of BC_{MA} and BP_M are partially disordered at their ends; the phytyl chains of BC_{LA} and BP_L have a different conformation and are well ordered. The carotenoid near BC_{MA} may contribute to this difference in phytyl chain structure since its presence prevents an identical arrangement of phytyl chains on both sides.

A measure of the rigidity of the structure are the atomic *B* values obtained during crystallographic refinement. These values are higher in the M-branch than in the L-branch. An example is the tetrapyrrole ring of BP_M, with an average *B* of 21.1 $Å^2$, as compared with 10.3 $Å^2$ for BP_L.

A major source of asymmetry are the protein subunits L and M surrounding the core pigments. Their overall sequence homology is only 25% (Michel *et al.*, 1986a). Although key residues like the histidines that are ligands to the Mg^{2+} ions of the BChl-bs, and to the non-haem iron are strictly conserved, most of the residues in contact with the core pigments are different between the two branches.

I now describe details of the protein environment of the pigments along the pathway of the electron, and mention additional differences between the branches that may be functionally important. Figure 13 shows a close view of the structures that are directly involved in the first step of the light-driven electron transfer reaction: the special pair, the accessory BChl-b BC_{LA} and the first electron acceptor, BP_L. In addition, a few amino acid residues in close contact to these pigments are shown. BC_{LA} is in Van der Waals contact with both the special pair and BP_L. The closest approach between the tetrapyrrole rings of the special pair and BP_L in 10 Å (atoms in double bonds). The phytyl chain of BC_{LP} follows a cleft formed by BC_{LA} and BP_L; it is in Van der Waals contact to both tetrapyrrole rings. At first glance this arrangement suggests that the electron should follow the path $P \rightarrow BC_{LA} \rightarrow BP_L$. However, attempts to observe bleaching of the absorption bands of BC_{LA} due to transient reduction failed. Spectroscopic experiments done with ultrafast laser systems indicated direct reduction of BP_L from P* without intermediate steps (Breton *et al.*, 1986; Fleming *et al.*, 1988; Kirmaier *et al.*, 1985b). This result has initiated an intense debate on the mechanism of electron transfer from P to BP_L, and on the role of BC_{LA} in this process. As indicated in Figure 13 with the example of tyrosine M208, it seems plausible that the protein plays an important role, not only as a scaffold to keep pigments in place, but also in influencing functional properties.

Numerous protein−pigment interactions are apparent also for the special pair itself (Michel *et al.*, 1986b), as shown in Figure 14. These interactions include bonds between Nε atoms of histidines L173 and M200 to the Mg^{2+} ions of BC_{LP} and BC_{MP} respectively. Both acetyl groups of the special pair are hydrogen bonded: BC_{LP} to histidine L168, and BC_{MP} to tyrosine M195. A further hydrogen bond is found between the ring V keto carbonyl oxygen and threonine L248; there is no equivalent hydrogen bond for BC_{MP}.

The special pair environment is rich in aromatic residues: five phenylalanines, three tyrosines and three tryptophans are in direct contact with the tetrapyrrole rings of the special pair. Tyrosine L162 is located between the special pair and the closest haem group (HE3) of the cytochrome, and may play a role during reduction of P^+ by the cytochrome (Michel *et al.*, 1986b).

Figure 15 shows BP_L, the first electron acceptor, with its protein environment (Michel *et al.*, 1986b). The BPh-bs are held in their places by non-covalent interactions only. In the positions where histidine ligands of BChl-bs would be expected, we find leucine M212 for BP_L (see Figure 15) and methionine L184 for BP_M. BP_L forms two hydrogen bonds with the protein. The one between the ring V ester carbonyl group and tryptophan L100 has an equivalent in a hydrogen bond between BP_M and tryptophan M127. The other hydrogen bond, between the ring V keto carbonyl oxygen and glutamic acid L104 is unique for the L-branch; the residue on the M-side corresponding to glutamic acid L104 is valine M131. Glutamic acid L104 is conserved in all currently known sequences of RC L-subunits for purple bacteria. Its position in the electron transfer pathway strongly suggests that it is protonated; otherwise, the negative charge of the ionized glutamic acid side chain would make electron

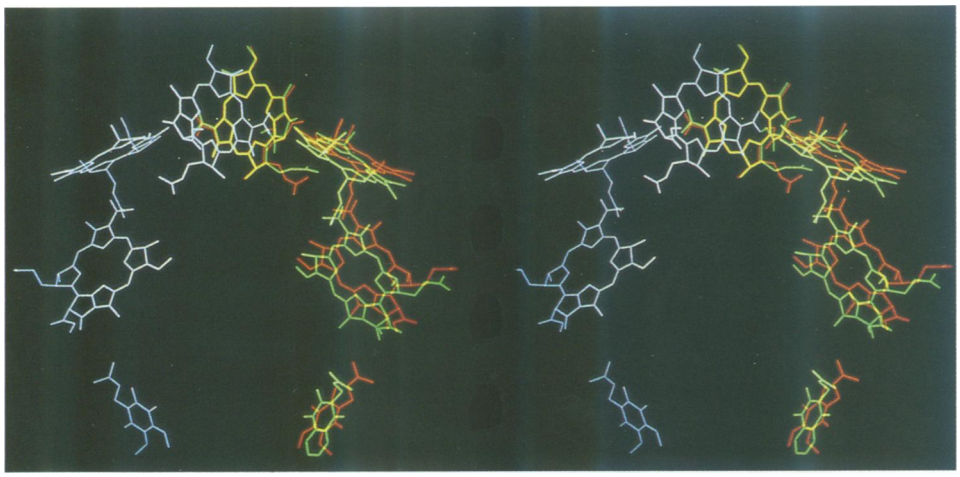

Fig. 12. Stereo pair showing cofactors of M-branch (purple), and of L-branch (green); phytyl chains are omitted for clarity. Red, cofactors of M-branch rotated using a transformation that optimally superimposes the tetrapyrrole ring of BC_{MP} onto that of BC_{LP}.

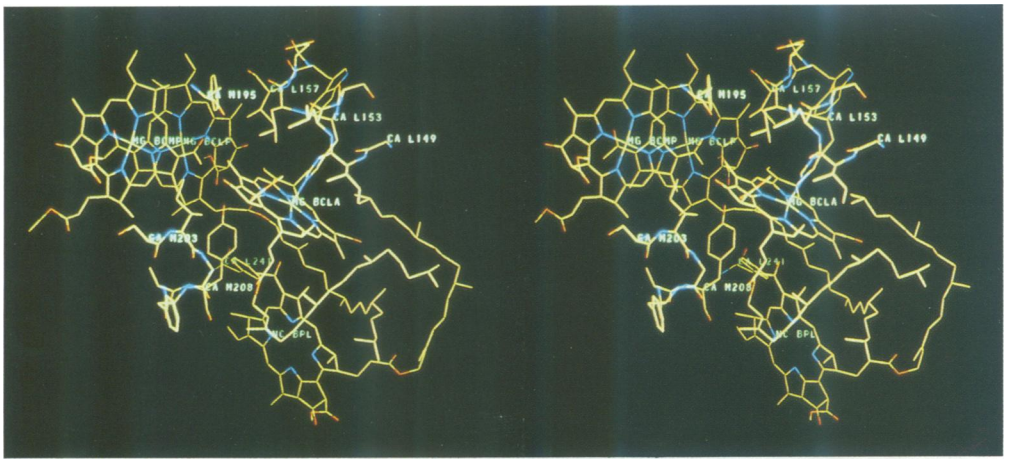

Fig. 13. Special pair, BC_{LA}, BP_L, and selected residues in atom colours.

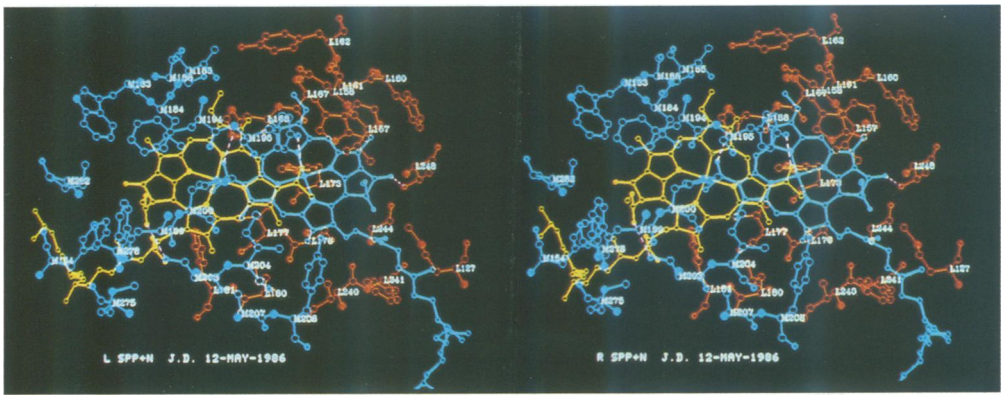

Fig. 14. Stereo pair, showing the special pair, and its protein environment (Michel *et al.*, 1986b). Brown, residues from the L-subunit; blue, residues from the M-subunit; green, BC_{LP}; yellow, BC_{MP}. Hydrogen bonds are indicated in purple. The hydrogen bond between serine M203 and BC_{MP} is no longer present in the refined model.

transfer to BP_L energetically highly unfavourable.

As for the special pair, aromatic residues are found in the neighbourhood of the BPh-bs; the neighbourhood of BP_L is richer in aromatic residues than that of BP_M. An especially noteworthy aromatic residue is tryptophan M250 whose side chain forms a bridge between BP_L and the next electron acceptor, Q_A. The M-branch residue equivalent to tryptophan M250 is phenylalanine L216 which, due to the

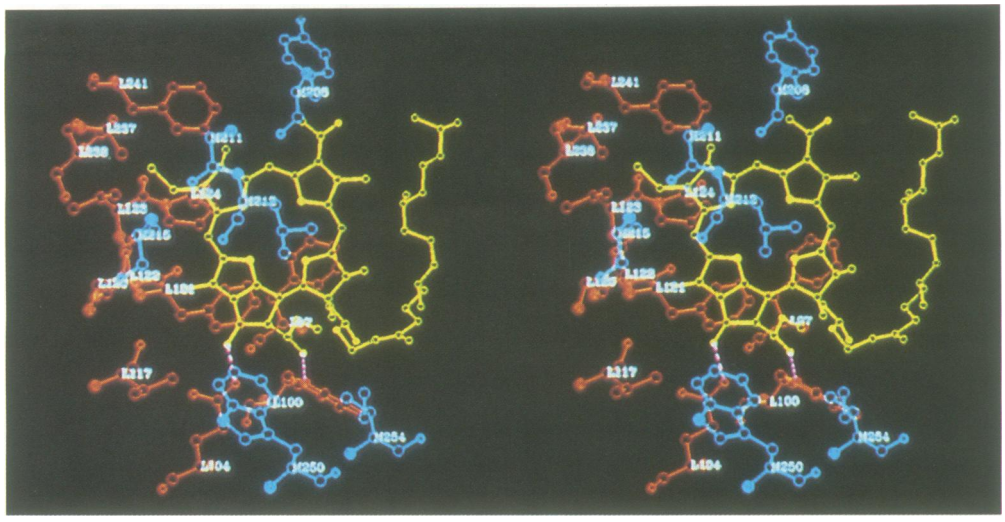

Fig. 15. Stereo pair, showing BP_L (yellow) and its protein environment, coloured as in Figure 14.

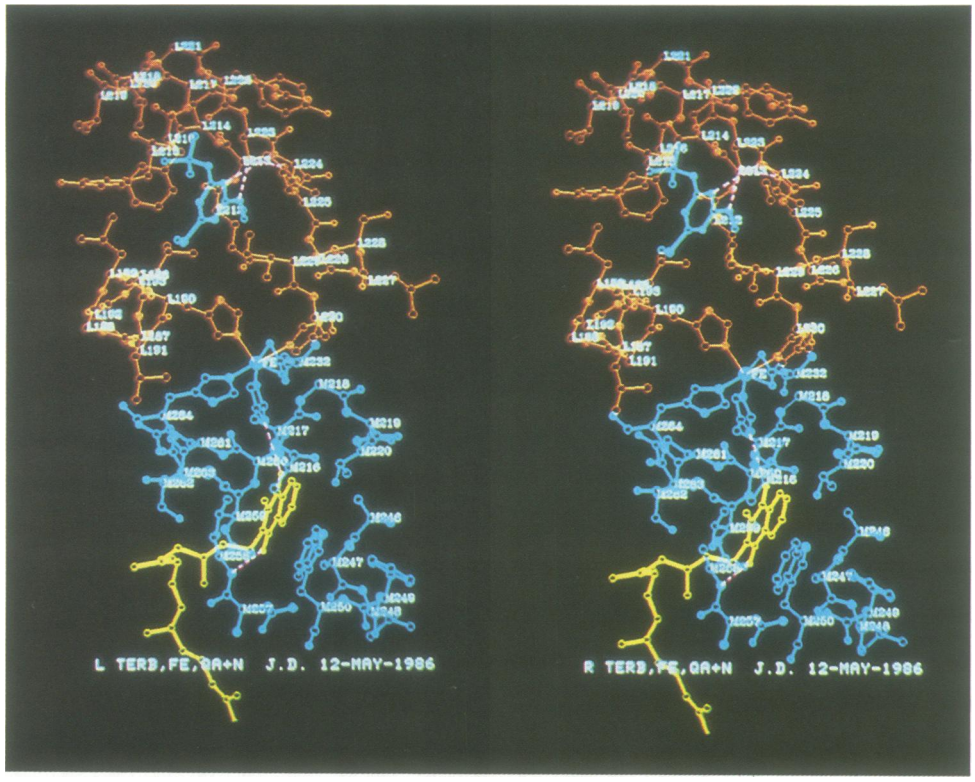

Fig. 16. Stereo pair, showing Q_A, the non-haem iron, the herbicide terbutryn in the Q_B binding pocket and the protein environment of these cofactors, coloured as in Figure 14 (Michel *et al.*, 1986b).

smaller side chain, cannot perform a similar bridging function between BP_M and Q_B.

The environment of the quinones, and of the non-haem iron (Michel *et al.*, 1986b) is shown in Figure 16. Instead of Q_B, the figure shows the herbicide terbutryn in the Q_B binding pocket. The non-haem iron appears in the centre of the drawing, between the binding sites of Q_A and Q_B, very near the central local 2-fold symmetry axis. It is bound by five protein side chains, four histidines (L190, L230, M217 and M264) and glutamic acid M232, whose carboxylate group acts as a bidentate ligand. The iron sits in a distorted octahedral environment with the axial ligands histidine L230 and histidine M264, and equatorial ligands histidine L190, histidine M217 and glutamic acid M232. Histidine L190 and histidine M217 also contribute significantly to the binding of Q_B and Q_A respectively. The location of the iron, and its binding to residues from subunits L and M immediately suggests that the part of the iron's role is to increase the structural stability of the RC. It is surprising that its role in electron transfer between the quinones seems to be relatively minor (Kirmaier *et al.*, 1986).

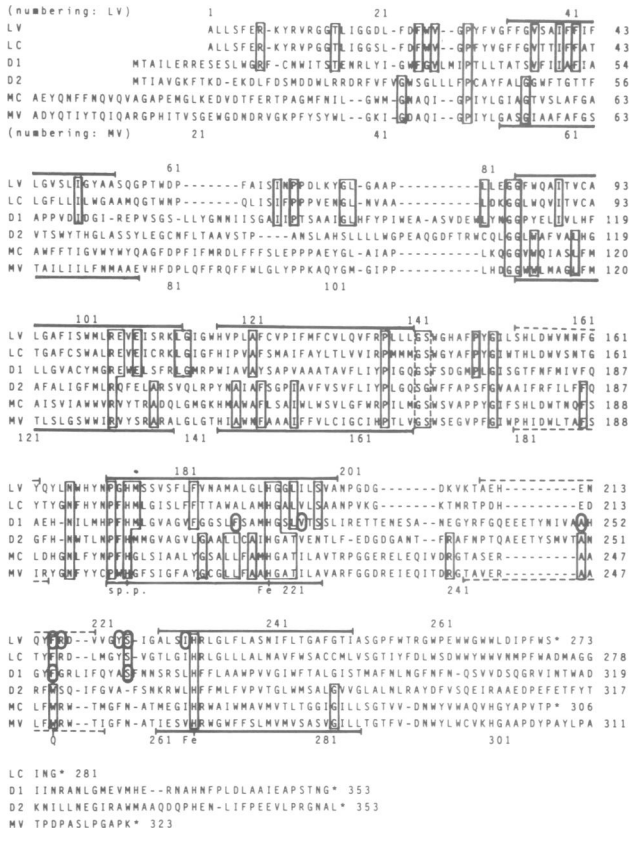

Fig. 17. The amino acid sequences of the L- and M-subunits from the purple bacteria *R. viridis* (LV, MV; Michel *et al.*, 1986a) and *R. capsulatus* (LC, MC; Youvan *et al.*, 1984). Amino acids common to all six subunits, the L-subunits and D1, or the M-subunits and D2 are boxed. The position of the transmembrane α-helices in the *R. viridis* RC is indicated by bars above the sequences of the L-subunits and below the sequences of the M-subunits. The positions of the short α-helices in the connections of transmembrane α-helices C and D, as well as D and E, are indicated by dashed lines. The histidine ligands of the special pair bacteriochlorophylls and of the non-haem iron atom are marked by sp.p. or Fe. Circles show amino acids known to be mutated in herbicide-resistant RCs from the purple bacteria or from PS II (taken from Michel and Deisenhofer, 1988).

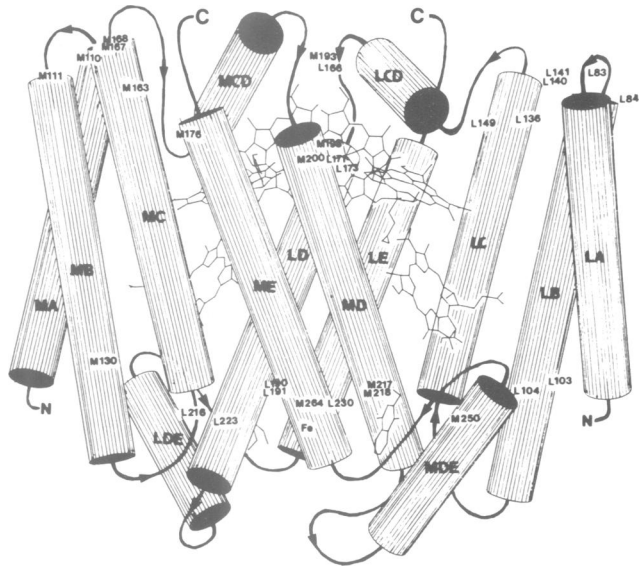

Fig. 18. Column model for the core of the RC from *R. viridis*. Only helices which are presumably conserved in PS II RCs are shown. The connections of the helices are only indicated schematically. The transmembrane helices of the L- (M-) subunit are labelled by LA-LE (MA-ME) and the major helices in the connections by LCD (MCD) and LDE (MDE). The special pair bacteriochlorophylls are at the interface of the L- and M- subunits between the D- and E-helices, the bacteriophaeophytins near the L-helices. The binding site for Q_A is between the LDE and LD helices. The location of the amino acids conserved between all L- and M-subunits and the D1 and D2 proteins, as well as those forming the quinone binding sites, is indicated by their sequence numbers (taken from Michel and Deisenhofer, 1988).

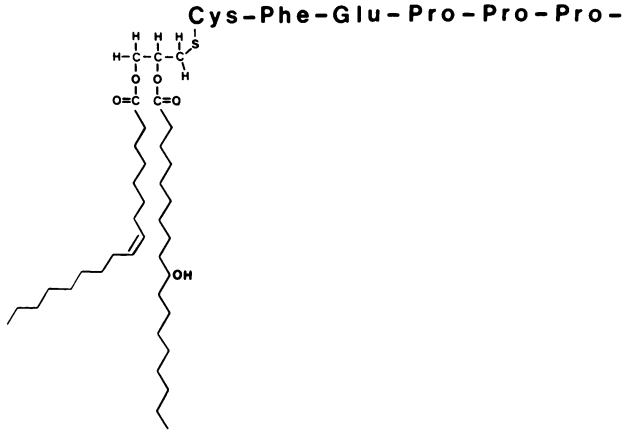

Fig. 19. The N-terminus of the cytochrome subunit. Two fatty acids are esterified to the N-terminal *S*-glycero-cysteine. The fatty acids are a mixture of 18:OH (two isomers) and 18:1 (three isomers) acids roughly in a 1:1 ratio, which are represented by oleic acid and 11-hydroxy-stearic acid in the figure (taken from Weyer *et al.*, 1987b).

The head group of Q_A is bound in a highly hydrophobic pocket; its carbonyl oxygens are hydrogen bonded to the peptide NH of Ala M258, and to the Nδ of the iron ligand histidine M217. As mentioned above, tryptophan M250 forms part of the Q_A's binding pocket; its indole ring is nearly parallel to the head group of Q_A at a distance of 2.1 Å. The isoprenoid side chain of Q_A is folded along the surface of the L−M complex; the last three isoprenoid units are disordered in the crystal. The Q_A binding pocket is well shielded from the cytoplasm by the globular domain of the H-subunit.

Since the Q_B binding site in the RC crystals is only partially occupied, the Q_B model is less reliable than the other parts of the structural model discussed above. Nevertheless, the crystallographic data suggested a highly plausible arrangement of the Q_B head-group in its pocket; the Q_B side chain remained undefined. It appears that Q_B, similar to Q_A, forms hydrogen bonds to the protein with its two carbonyl oxygens: one to Nδ atom of the iron ligand histidine L190, and a bifurcated hydrogen bond to Oγ of serine L223, and to NH of glycine L225. As tryptophan M250 for Q_A, phenylalanine L216 forms a significant part of the Q_B binding pocket. Major differences between the binding sites of Q_A and Q_B are the more polar nature of the Q_B site, and the presence of pathways through the protein, through which protons may enter the Q_B site. The bottom of the Q_B site is formed to a large part by the side chain of glutamic acid L212. Protons can move from the cytoplasm along a path marked by charged or polar residues to glutamic acid L212 and from there, by an as yet unknown mechanism, to the doubly reduced Q_B^{2-}.

Some herbicides are competitive inhibitors of Q_B binding to RCs of purple bacteria. Crystallographic binding studies with the herbicide terbutryn (see Figure 16) and with *o*-phenanthroline (Deisenhofer *et al.*, 1985a; Michel *et al.*, 1986b) demonstrated binding of these molecules in the Q_B binding pocket, and provided a structural basis for understanding mutations that render *R. viridis* herbicide resistant (Sinning and Michel, 1987a,b). The fact that herbicides which were developed to inhibit photosystem II RCs of green plants, can also inhibit RCs of purple bacteria is one of the many indications of a close structural similarity between these kinds of photosynthetic RC [see Section 4 and Michel and Deisenhofer (1988)].

4. The relation to photosystem II and evolutionary aspects

4.1. *Conclusions on the structure of photosystem II RC*

The most surprising result of the X-ray structure analysis was the discovery of the nearly symmetrical arrangement of the RC core formed by the homologous L- and M-subunits together with the pigments. Primary electron donor as well as the ferrous non-haem iron atom are found at the interface between both subunits. Both subunits are needed to establish the RC.

During the X-ray structure analysis the following results suggesting a close relationship between the RCs from purple bacteria and photosystem II (PS II) were, or became, available. (i) PS II RC and the RC from purple bacteria both possess two pheophytin molecules (Omata *et al.*, 1984; Feher and Okamura, 1978). Upon removal of the quinones or prereduction of them it is possible to trap one electron on one of them (Shuvalov and Klimov, 1976; Tiede *et al.*, 1976). (ii) Both RCs possess a magnetically coupled Q_A-Fe-Q_B complex. (iii) The L-subunit of the purple RC and the D1 protein (which is the product of the *psbA* gene and also called Q_B protein, 32-kd protein or herbicide-binding protein) bind the herbicide azidoatrazine upon photoaffinity labelling (Pfister *et al.*, 1981; de Vitry and Diner, 1984). (iv) Weak but significant sequence homologies between the L- and M-subunits of the purple bacteria (Williams *et al.*, 1983, 1984; Youvan *et al.*, 1984; Michel *et al.*, 1986a), the D1 (Zurawski *et al.*, 1982) and later on also D2 proteins (Alt *et al.*, 1984; Holschuh *et al.*, 1984;

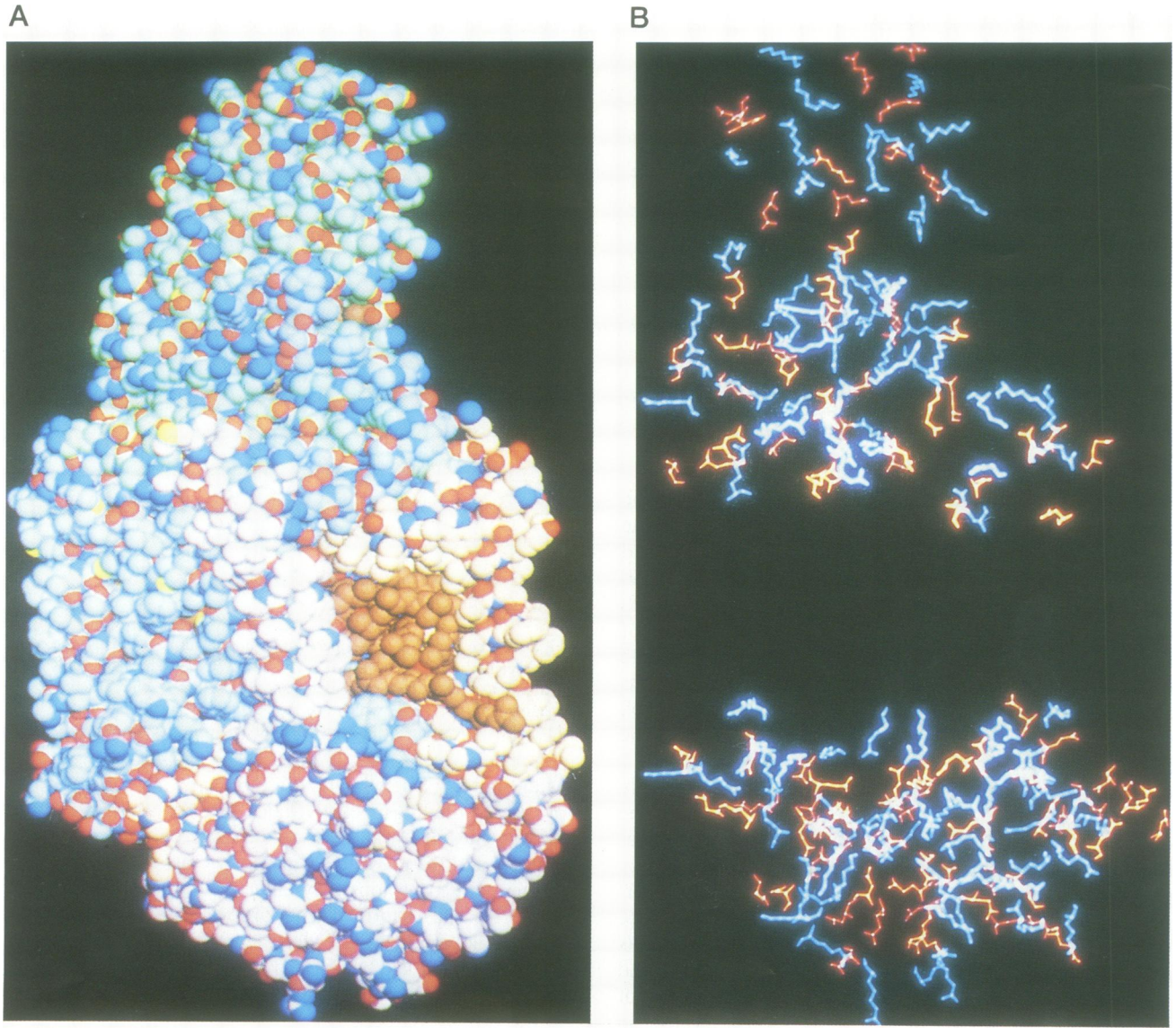

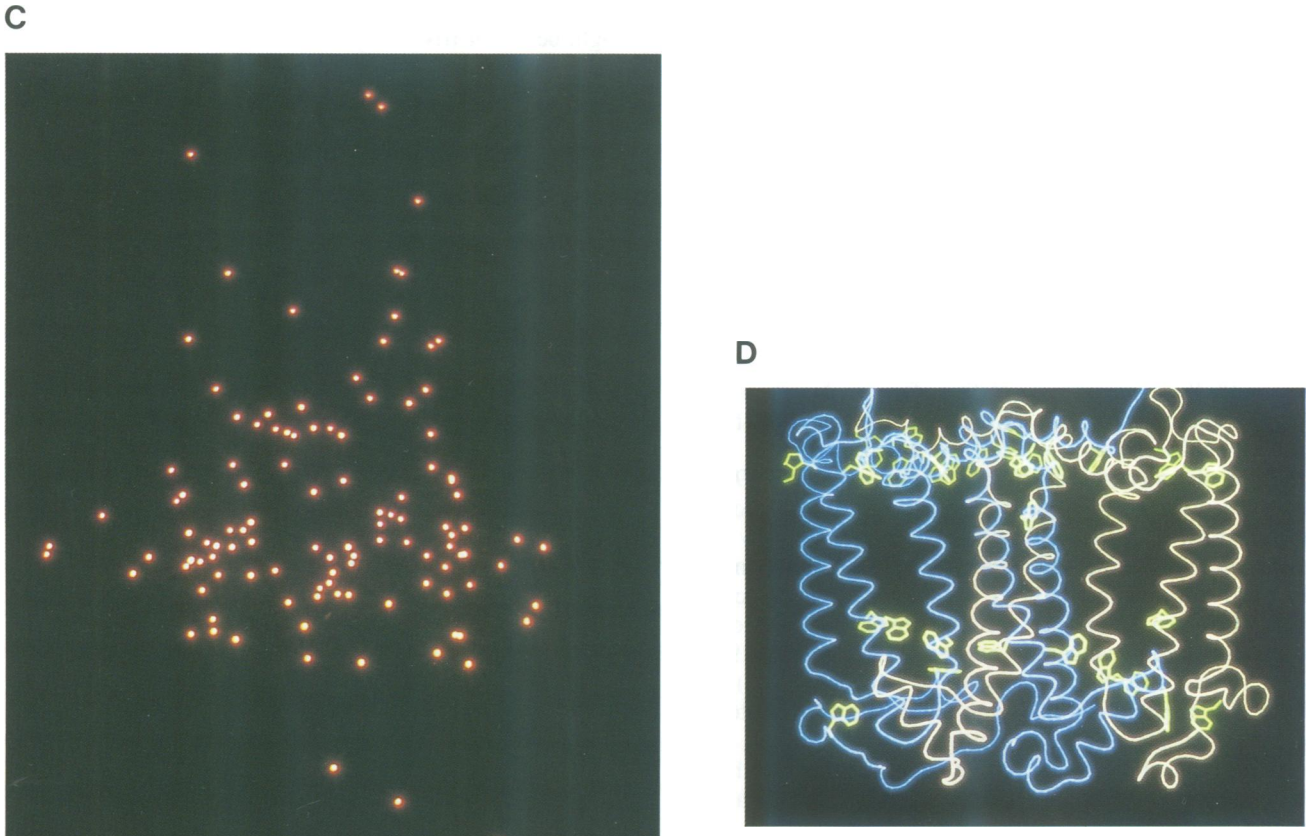

Fig. 20. (**A**) Space filling model of the photosynthetic RC from *R. viridis*. Carbon atoms are showed in white, nitrogen atoms in blue, oxygen atoms in red and sulphur in yellow. The visible atoms of a bacteriophaeophytins approaching the surface are represented in brown. (**B**) Distribution of the 'charged' amino acids in the photosynthetic reaction centre from *R. viridis*. The negatively charged amino acids (aspartate and glutamate) are shown in red, the positively charged amino acids (arginine and lysine) in blue. (**C**) Distribution of bound water molecules in the RC. The RC and the L- and M-subunits are always shown from a view parallel to the membrane. (**D**) Distribution of trypotophan residues (green) in the L- (brownish) and M-subunits (blue).

Rasmussen *et al.*, 1984; Rochaix *et al.*, 1984) of PS II were discovered.

The meaning of the results was obvious. The RC of PS II from plants and algae was expected to be formed by the D1 and D2 proteins with D1 corresponding to the L-subunit and D2 corresponding to the M-subunit. This proposal was at variance with the accepted view that the so-called CP47, a chlorophyll-binding protein with apparent mol. wt of 47 000, is the apoprotein of the PS II RC (Nakatani *et al.*, 1984).

Figure 17 compares the amino acid sequences of the L- and M-subunits from two purple bacteria with the D1 and D2 proteins from spinach chloroplasts. Significant sequence homology starts with the glycine–glycine pair (L83,84 M 110,111) at the beginning of the second transmembrane helices. Mainly amino acids of structural importance such as glycines, prolines and arginines are conserved. Part of the amino acids involved in the binding of the pigments and cofactors are also conserved: the histidine ligands to the magnesium atoms of the special pair chlorophylls (L173, M200) and to the non-haem iron atom. In the L-subunit and the D1 protein a phenylalanine residue (L216, D1-255) and a serine residue (L223, D1-264) are found in the corresponding sequence positions. These residues are involved in the binding of the *s*-triazine herbicides, e.g. atrazine and terbutryn, which presumably act by competing with the secondary quinone Q_B for its binding site. Mutations of these amino acids cause herbicide resistance in the purple bacteria, in plants and algae. The phenylalanines L216 and D1-255 correspond to tryptophans M250 and D2-254 which form the major part of the binding site of the primary quinone Q_A.

Several important differences exist between the RCs of PS II and the purple bacteria: the amino acids involved in the binding of the accessory bacteriochlorophylls in the purple bacteria, and a glutamic acid which is a bidentate ligand to the ferrous non-haem iron are not conserved. There is no hint of the existence of an analogue to the H-subunit in PS II RC. The overall structure of the PS II RC core, however, must be very similar to the RC from purple bacteria formed by the L- and M-subunits. Figure 18 shows those helices which are presumably conserved between the

RC cores of the purple bacteria and PS II and the position of the amino acids conserved between the L- and M-subunits and the D1 and D2 proteins. Identity between amino acids which are found specifically in the L-subunits and the D1 proteins, or specifically in the M subunits and D2 proteins, and involved in the quinone binding, might be the result of convergent evolution. Their location is also shown.

The rereduction of the photooxidized primary electron donor occurs from the cytochrome subunit in the RC from *R.viridis*. In the position equivalent to the cytochrome subunit we have to expect the water-soluble proteins forming part of the manganese-containing oxygen-evolving complex in the PS II RC. Experimental proof for the existence of a similar RC core in PS II was the recent isolation of a complex consisting of the proteins D1 and D2 and cytochrome b_{559} from spinach chloroplasts, which contained four to five chlorophylls and two pheophytins (Nanba and Satoh, 1987). It has been shown to be active in electron transport to the pheophytins. Recently evidence has been presented by two groups that a tyrosine residue located on the D1 subunit in the third transmembrane helix is an intermediate electron carrier between the primary electron donor of PS II and the oxygen-evolving manganese cluster (Debus *et al.*, 1988; Vermaas *et al.*, 1988; Hoganson and Babcock, 1988). At present it is speculated that even the manganese cluster is bound to the D1 and D2 proteins.

As a result of the work on the bacterial photosynthetic RC our entire view of the PS II RCs from plants and algae has changed.

4.2. *Evolutionary aspects*

The sequence similarities discussed above suggest that the RCs from purple bacteria and PS II are evolutionarily related. A common ancestor possessed an entirely symmetrical RC with two parallel electron-transporting pigment branches across the membrane. In this view the symmetrical RC was formed by two copies of the same protein subunit encoded by one gene. After a gene duplication and subsequent mutations the formation of the asymmetrical dimer and the use of only one pigment branch for electron transfer became possible. It is an open question if in evolution this gene duplication occurred only once, before the lineages leading to the purple bacteria and the PS II containing organisms split, or twice, after the splitting into these two lineages. In the latter case the specific sequence similarities between L and D1, as well as those between M and D2, would be the result of convergent evolution, whereas the identities of the structurally important amino acids would date back to the original symmetrical dimer. Sequence comparisons are in favour of the latter possibility (see Williams *et al.*, 1986): the sequence identity between the D1 and D2 proteins is much higher than those between the L- and M-subunits. This observation possibly indicates that the gene duplication giving rise to separate D1 and D2 proteins occurred later during evolution than the gene duplication leading to the L- and M-subunits. On the other hand, due to more and stronger interactions with neighbouring proteins, the D1 and D2 proteins had less freedom to mutate than the L- and the M-subunits. As a result sequence comparisons might be misleading.

The evolutionary relationships also indicate that there must be an advantage for RCs possessing only one active electron transport chain with two quinones acting in series. There might be rather trivial explanations for the use of only one branch, e.g. an asymmetry in the protein environment can cause an asymmetry in the distribution of electrons in the excited state and subsequently lead to a preferred release of an electron only in one direction. This existing polarity might lead to a faster rate of the first electron transfer step, a minimization of competing reactions and thus a higher quantum yield for the electron transfer.

It is a clear advantage in the present day's RCs that the two quinones act in series, and only the released secondary quinone, Q_B, is a two-electron carrier. Consider the situation of the ancient symmetrical RC. Upon the first excitation the electron is transferred to the quinone at the end of one pigment branch. The resulting semiquinone is not stable and its electron is lost in the time range of seconds. Only if it receives a second electron can it be protonated and energy stored in the form of the quinol. With two identical parallel electron-transfer chains the probability that the second electron will be funnelled into the same chain, to the same quinone, as the first electron is only 50%. A possible electrostatic repulsion by the negatively charged semiquinone might even decrease this probability. Frequently, the absorption of the two photons leads to the formation of two semiquinones in the same RC and energy is not stored in a stable way. The way out of this dilemma clearly is to switch the two quinones in series, and to allow protonation and release only to the final quinone, which is then Q_B in the electron-transfer chain, as it is seen in the RCs of purple bacteria and PS II. A considerable increase in the efficiency of light-energy conversion, especially under low light conditions, must result.

5. Aspects of membrane protein structure

5.1. *The membrane anchor of the cytochrome subunit*

The X-ray structure analysis established that the L- and M-subunits are firmly integrated into the membrane, both possessing five transmembrane helices, whereas the H-subunit is anchored to the membrane by one transmembrane helix. The X-ray work showed no indication of any intramembranous part of the cytochrome subunit. Nevertheless, in the hands of the biochemists it behaved like a membrane protein and aggregated easily. A strange observation during the protein sequencing was that upon Edman-degradation of the isolated cytochrome subunit no N-terminal amino acid could be identified after the first degradation, but a normal sequence could be obtained starting with the second amino acid from the N-terminus. K.A.Weyer was then able to isolate a modified N-terminal amino acid with the help of F.Lottspeich, and to elucidate the structure of this modified N-terminal amino acid together with W.Schäfer using mass spectrometry (Weyer *et al.*, 1987a,b). The result is shown in Figure 19. The N-terminal amino acid is a cysteine linked to a glycerol residue via a thioether bridge. Two fatty acids are then esterified to the two OH-groups of the glycerol. The fatty acids are a statistical mixture of singly unsaturated C_{18} fatty acids and singly hydroxylated C_{18} fatty acids. These experiments firmly established that the cytochrome subunit also possesses a membrane anchor, but this is of a lipid type and not of a peptide type. The membrane anchor is very similar to that of the bacterial lipoproteins (see, for example, Pugsley *et al.*,

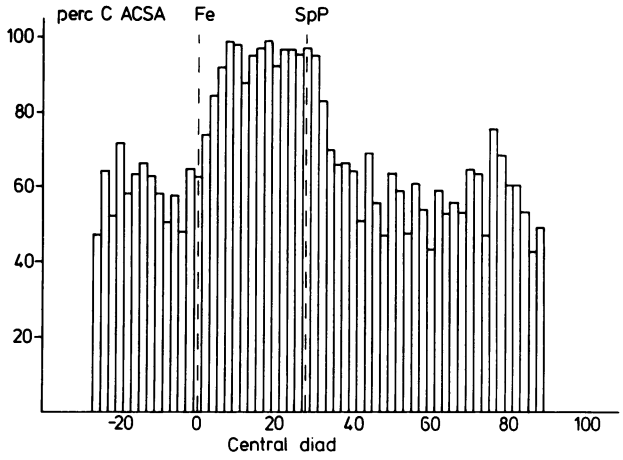

Fig. 21. Percentage (perc) of the accessible surface area (ACSA) occupied by carbon atoms shown for 3 Å thick layers perpendicular to the non-crystallographic 2-fold rotation axis, which runs through the ferrous non-haem-iron atom (Fe) and the special pair (Sp P).

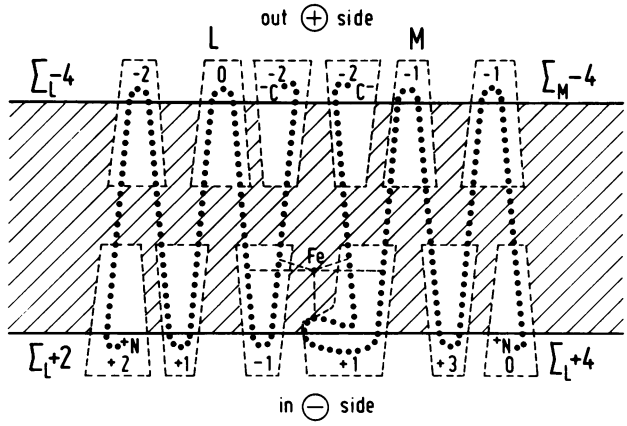

Fig. 22. Schematic drawing of the transmembrane helices and the helix connections of the L- and M-subunits from the *R. viridis* RC in the membrane to show the net charges at the ends of the helices and the helix connections. The negatively charged interior of the cell is indicated by the minus sign at the bottom, the positively charged extracellular medium by the plus sign at the top (taken from Michel and Deisenhofer, 1987).

1986; Yu *et al.*, 1986). The RC cytochrome subunit is the first cytochrome molecule known to contain such a membrane anchor.

5.2. *Protein lipid contacts*

The contact between lipids and protein occurs at the surface of the proteins. Therefore a look on the surface of the protein complex might be very informative. For this purpose a space-filling model of the RC is shown as Figure 20A. Carbon atoms approaching the surface of the RC are shown as white spheres. A central section perpendicular to the ~2-fold rotation axis can be seen where carbon atoms form the surface of the protein almost exclusively. They are mainly side chain atoms of the amino acids leucine, isoleucine and phenylalanine. This central zone must correspond to the hydrophobic part of the protein surface which in the membrane is in contact with the alkane chains of lipids. Approaching the cytoplasmic rim of the central zone a row

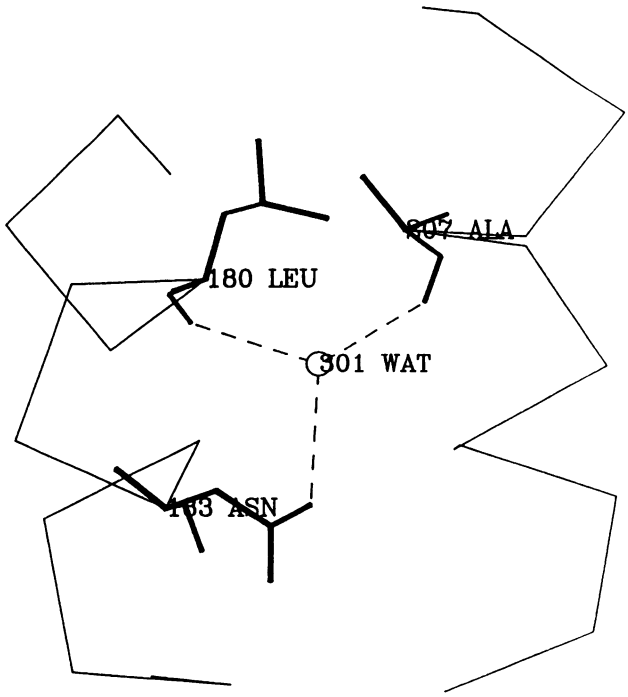

Fig. 23. A firmly bound water molecule (301 WAT) in the hydrophobic part of the membrane crosslinking two transmembrane helices by forming hydrogen bonds with the peptide oxygen atoms of leucine L180 and alanine M207. Another hydrogen bond with the side chain of asparagine L183 is possible.

of nitrogen atoms is seen at the protein surface. These nitrogen atoms are side chain atoms of the basic amino acids, arginine and histidine. The role of these basic residues might be to determine the position of the RC perpendicular to the membrane via specific interactions between negatively charged phosphate groups of the lipids and the positively charged amino acid side chains of the RC protein subunits

Figure 21 presents the percentage of the 'accessible surface area' which is covered by carbon atoms, shown in layers perpendicular to the central 2-fold rotation axis. The 2-fold rotation axis runs through the non-haem iron atom near the cytoplasmic side and relates the special pair bacteriochlorophylls near the periplasmic side of the membrane. Two important conclusions can be drawn from Figure 21. (i) The primary electron donor (special pair), is located in the hydrophobic non-polar part of the membrane, whereas the non-haem iron atom is already in that zone where the protein surface is polar and most likely interacts with the polar head-groups of the lipids. (ii) The thickness of the hydrophobic zone perpendicular to the membrane is 30–31 Å only. This value is smaller than expected for a lipid bilayer composed of lipids with C_{18} fatty acids.

5.3. *Distribution of amino acids and bound water molecules*

Figure 20B shows the distribution of the strongly basic amino acids, arginine and lysine, and of the strongly acidic amino acids, glutamic acid and aspartic acid, which, at neutral pH, possess electric charges at the ends of their side chains. A central zone, where none of these amino acids is found, has a thickness of ~25 Å and is thus slightly thinner than the hydrophobic surface zone shown in Figures 20 and 21. The slight discrepancy is due to two arginine residues and one

glutamic acid residue, which are apparently in a hydrophobic environment without counter charges. The role of the positive charges of the arginine side chains seems to be structural. They possibily cancel the partial negative charge at the C-terminal ends of the short helices in the connections of the long C and D transmembrane helices. These short helices partly intrude into the hydrophobic zone of the membrane and a positive charge seems to be necessary for the change of the direction of the peptide chain. The glutamic acid (L104) seems to be protonated, thus neutral, and to form a hydrogen bond with one of the bacteriopheophytins (Michel *et al.*, 1986b).

Within the L- and M-subunits the glutamates and aspartates, and the lysine and arginine residues, show an interesting asymmetrical distribution with respect to cytoplasmic and periplasmic sides. If one calculates 'net charges' of the peptide chains on the periplasmic side of the membrane and compares them with the net charges of the cytoplasmic side (assuming that all glutamic acid residues, aspartic acid residues and the C-termini are negatively charged, whereas all the arginine and lysine residues and the N-termini are positively charged) one finds that the cytoplasmic ends of the transmembrane helices and their respective connections are nearly always less negatively charged than their counterparts on the periplasmic side. This phenomenon is illustrated schematically in Figure 22. As a result the cytoplasmic part of the M-subunit carries four positive net charges and the periplasmic part four negative charges, the cytoplasmic part of the L-subunit two positive charges and the periplasmic part four negative charges. The charge asymmetry becomes even more pronounced if one considers the existence of the firmly bound non-haem iron atom on the cytoplasmic side and the presumed protonation of glutamic acid L104. Thus these membrane proteins are strong electric dipoles. This result can be correlated with the fact that the interior of bacteria is negatively charged, due to the action of electrogenic ion pumps. This means that the L- and M-subunits are orientated in the membrane in the energetically more favourable manner. *Vice versa*, the combination of the electric field across the membrane, established by the ion pumps, and the anisotropic distribution of negatively and positively charged amino acids in the protein may be one of the factors which determine the orientation of membrane proteins with respect to the inside and outside of the cell.

In the L- and M-subunits the remarkably uneven distribution of the amino acid tryptophan as shown in Figure 20C was quite unexpected. About two thirds of the tryptophans are found at the ends of transmembrane helices or in the helix connections on the periplasmic site. Only a few tryptophan residues are seen in the hydrophobic zone, where they are in contact with pigments. The residual tryptophans are located in the hydrophobic surface-to-polar transition zone or the polar part of the L- and M-subunits near the cytoplasmic hydrophobic surface. The indole rings of the tryptophans are orientated preferentially towards the hydrophobic zone of the membrane.

Figure 25D shows the distribution of the bound water molecules which have been tentatively identified by the X-ray crystallographic analysis. Only five of them are found in the hydrophobic intramembranous zone. A closer inspection shows that they may perform an important structural role. Figure 23 shows one of these water molecules and its probable hydrogen-bonding pattern. It apparently crosslinks two transmembrane helices, one of the L-subunit, the other of the M-subunit by donating hydrogen bonds to two peptide oxygen atoms. Another hydrogen bond with an asparagine side chain is possible. How much these water molecules contribute to the stability of the RC structure has to be determined in the future.

5.4. *Crystal packing and detergent binding*

As outlined in Section 1 the most promising strategy was to crystallize the RCs within the detergent micelles. According to this concept the crystal lattice should be formed by polar interactions between polar surface domains of the RC. This expectation was confirmed by the results of the structural analysis. Mainly the polar surfaces of the cytochrome subunit and the H-subunit are involved in the crystal packing, to a minor extent also the polar surface part of the M-subunit.

As expected for detergents in a micelle most of the detergent is crystallographically not ordered and cannot be seen in the electron density map, with one exception. The single transmembrane helix of the H-subunit, two transmembrane helices of the M-subunit, and part of the pigments seem to form a pocket where one detergent molecule is bound. Its polar head-group apparently undergoes specific interactions with the protein near the cytoplasmic end of the hydrophobic surface zone. Specific binding of this particular detergent molecule might explain why crystals of the photosynthetic RC from *R. viridis* could be grown only with *N,N*-dimethyldodecylamine-*N*-oxide as detergent, but not when octylglucopyranoside or similar detergents were used.

In collaboration with M.Roth and A.Bentley-Lewis from the Institut Laue-Langevin in Grenoble the detergent micelle could be visualized by neutron crystallography and H_2O/D_2O contrast variation. A rather flat, monolayer-like ring of detergent molecules surrounding the hydrophobic surface zone of the RC became visible. Regions where the detergent micelles are in contact can also be seen. Therefore, attractive interactions between detergent micelles may also contribute to the stability of the protein's crystal lattice. In general, the strategy to crystallize membrane proteins within their detergent micelles (Michel, 1983; Garavito *et al.*, 1986) now seems to be proven. However, the progress made in crystallizing membrane proteins, other than bacterial photosynthetic RCs and bacterial porins, has been unexpectedly slow: well diffracting crystals of membrane proteins have only been obtained in these cases. The necessary fine tuning with respect to the size of the detergent micelle and the size of the polar head group of the detergent still is a formidable task which has to be solved empirically for each individual membrane protein.

Acknowledgements

We wish to express our sincere gratitude to persons and organizations who helped to make our work possible and successful. Our colleagues Otto Epp, Heidi Grünberg, Friedrich Lottspeich, Kunio Miki, Wolfram Schäfer, Irmgard Sinning, Karl-Alois Weyer and Wolfgang Zinth made improtant direct contributions as mentioned in the text. Dieter Oesterhelt and Robert Huber, their departments and the whole Max-Planck-Institut für Biochemie provided facilities and a stimulating and supportive atmosphere. Dieter Oesterhelt's backing, especially during the initial, frustrating phases, and the stable environment in the Max-Planck-Gesellschaft allowed a project

of unknown duration and outcome to start. Financially the project was supported by the Deutsche Forschungsgemeinschaft through Sonderforschungsbereich 143 (Teilprojekt A3 to H.M., Teilprojekt A6 to J.D. and H.M.) and the Max-Planck-Gesellschaft.

References

Allen,J.P. and Feher,G. (1984) *Proc. Natl. Acad. Sci. USA*, **81**, 4795–4799.

Allen,J.P., Feher,G., Yeates,T.O., Rees,D.C., Deisenhofer,J., Michel,H. and Huber,R. (1986) *Proc. Natl. Acad. Sci. USA*, **83**, 8589–8593.

Alt,J., Morris,J., Westhoff,I. and Herrmann,R.G. (1984) *Curr. Genet.*, **8**, 597–606.

Baumeister,W. and Vogell,W. (eds) (1980) *Electron Microscopy at Molecular Dimensions*. Springer, Berlin.

Bjorkmann,P.J., Saper,M.A., Samraoui,B., Bennett,W.S., Strominger,J.L. and Wiley,D.C. (1987) *Nature*, **329**, 506–512.

Breton,J., Martin,J.L., Migus,A., Antonetti,A. and Orszag,A. (1986) *Proc. Natl. Acad. Sci. USA*, **83**, 5121–5125.

Chang,C.H., Schiffer,M., Tiede,D., Smith,U. and Norris,J. (1985) *J. Mol. Biol.*, **186**, 201–203.

Chang,C.H., Tiede,D., Tang,J., Smith,U., Norris,J. and Schiffer,M. (1986) *FEBS Lett.*, **205**, 82–86.

Clayton,R.K. and Clayton,B.J. (1978) *Biochim. Biophys. Acta*, **501**, 478–487.

de Vitry,C. and Diner,B. (1984) *FEBS Lett.*, **167**, 327–331.

Debus,R.J., Feher,G. and Okamura,M.Y. (1986) *Biochemistry (Wash.)*, **25**, 2276–2287.

Debus,R.J, Barry,B.A., Babcock,G.T. and McIntosh,L. (1988) *Proc. Natl. Acad. Sci. USA*, **85**, 427–430.

Deisenhofer,J., Epp,O., Miki,K., Huber,R. and Michel,H. (1984) *J. Mol. Biol.*, **180**, 385–398.

Deisenhofer,J., Epp,O., Miki,K., Huber,R. and Michel,H. (1985a) *Nature*, **318**, 618–624.

Deisenhofer,J., Remington,S.J. and Steigemann,W. (1985b) *Methods Enzymol.*, **115**, 303–323.

Deisenhofer,J. and Michel,H. (1988) In Breton,J. and Vermeglio,A. (eds), *The Photosynthetic Bacterial Reaction Center Structure and Dynamics*. Plenum Press, New York, pp. 1–3.

Dracheva,S.M., Drachev,L.A., Konstantinov,A.A., Semenov,A.Y., Skulachev,V.P., Arutijunjan,A.M., Shuvalov,V.A. and Zaberezhnaya,S.M. (1988) *Eur. J. Biochem.*, **171**, 253–264.

Feher,G. and Okamura,M.Y. (1978) In Clayton,R.K. and Sistrom,W.R. (eds), *The Photosynthetic Bacteria*. Plenum Press, New York, London, pp. 349–386.

Fleming,G.R., Martin,J.L. and Breton,J. (1988) *Nature*, **333**, 190–192.

Garavito,R.M. and Rosenbusch,J.P. (1980) *J. Cell Biol.*, **86**, 327–329.

Garavito,R.M., Markovic-Housley,Z. and Jenkins,J.A. (1986) *J. Crystal Growth*, **76**, 701–709.

Gast,P., Michalski,T.J., Hunt,J.E. and Norris,J.R. (1985) *FEBS Lett.*, **179**, 325–328.

Henderson,R. and Unwin,P.N.T. (1975) *Nature*, **257**, 28–32.

Hoganson,C.W. and Babcock,G.T. (1988) *Biochemistry (Wash.)*, **27**, 5848–5855.

Holschuh,K., Bottomley,W. and Whitfield,P.R. (1984) *Nucleic Acid Res.*, **12**, 8819–8834.

Happe,M. and Overath,P. (1976) *Biochem. Biophys. Res. Commun.*, **72**, 1504–1511.

Henderson,R. and Unwin,P.N.T. (1975) *Nature*, **257**, 28–32.

Hoganson,C.W. and Babcock,G.T. (1988) *Biochemistry (Wash.)*, **27**, 5848–5855.

Holschuh,K., Bottomley,W. and Whitfield,P.R. (1984) *Nucleic Acid Res.*, **12**, 8819–8834.

Huber,R., Schneider,M., Epp,O., Mayr,I., Messerschmidt,A., Pflugrath,J. and Kayser,H. (1987) *J. Mol. Biol.*, **195**, 423–434.

Jack,A. and Levitt,M. (1978) *Acta Crystallogr., A*, **34**, 931–935.

Jones,T.A. (1978) *J. Appl. Crystallogr.*, **11**, 268–272.

Jones,T.A., Bartels,K. and Schwager,P. (1977) In Arndt,U.W. and Wonacott,A.J. (eds) *The Rotation Method in Crystallography*. North Holland, Amsterdam, pp. 105–117.

Kirmaier,C. and Holten,D. (1987) *Photosynthesis Res.*, **13**, 225–260.

Kirmaier,C., Holten,D. and Parson,W.W. (1985a) *Biochim. Biophys. Acta*, **810**, 33–48.

Kirmaier,C., Holten,D. and Parson,W.W. (1985b) *Biochim. Biophys. Acta*, **810**, 49–61.

Kirmaier,C., Holten,D., Debus,R.J., Feher,G. and Okamura,M.Y. (1986) *Proc. Natl. Acad. Sci. USA*, **83**, 6407–6411.

Knapp,E.W., Fischer,S.F., Zinth,W., Sander,M., Kaiser,W., Deisenhofer,J. and Michel,H. (1985) *Proc. Natl. Acad. Sci. USA*, **82**, 8463–8467.

Lee,B. and Richards,F.M. (1971) *J. Mol. Biol.*, **55**, 379–400.

Luzzati,P.V. (1952) *Acta Crystallogr.*, **5**, 802–810.

Mathews,F.S., Argos,P. and Levine,M. (1972) *Cold Spring Harbor Symp. Quant. Biol.*, **36**, 387–397.

Michel,H. (1982a) *EMBO J.*, **1**, 1267–1271.

Michel,H. (1982b) *J. Mol. Biol.*, **158**, 567–572.

Michel,H. (1983) *Trends Biochem. Sci.*, **8**, 56–59.

Michel,H. and Deisenhofer,J. (1987) *Chem. Scripta*, **27B**, 173–180.

Michel,H. and Deisenhofer,J. (1988) *Biochemistry (Wash.)*, **27**, 1–7.

Michel,H. and Oesterhelt,D. (1980) *Proc. Natl. Acad. Sci. USA*, **77**, 1283–1285.

Michel,H., Oesterhelt,D. and Henderson,R. (1980) *Proc. Natl. Acad. Sci. USA*, **77**, 338–342.

Michel,H., Deisenhofer,J., Miki,K., Weyer,K.A. and Lottspeich,F. (1983) In Quagliariello,E. and Palmieri,F. (eds), *Structure and Function of Membrane Proteins*. Elsevier, Amsterdam, pp. 191–197.

Michel,H., Weyer,K.A., Gruenberg,H. and Lottspeich,F. (1985) *EMBO J.*, **4**, 1667–1672.

Michel,H., Weyer,K.A., Gruenberg,H., Dunger,I., Oesterhelt,D. and Lottspeich,F. (1986a) *EMBO J.*, **5**, 1144–1158.

Michel,H., Epp,O. and Deisenhofer,J. (1986b) *EMBO J.*, **5**, 2445–2451.

Michel-Beyerle,M.E., Plato,M., Deisenhofer,J., Michel,H., Bixon,M. and Jortner,J. (1988) *Biochim. Biophys. Acta*, **932**, 52–70.

Nakatani,H.Y., Ke,B., Dolan,E. and Arntzen,C.J. (1984) *Biochim. Biophys. Acta*, **765**, 347–352.

Nanba,O. and Satoh,K. (1987) *Proc. Natl. Acad. Sci. USA*, **84**, 109–112.

Newcomer,M.E., Jones,T.A., Aqvist,J., Sundelin,J., Eriksson,U., Rask,I. and Peterson,P.A. (1984) *EMBO J.*, **3**, 1451–1454.

Norris,J.R., Uphaus,R.A., Crespi,H.L. and Katz,J.J. (1971) *Proc. Natl. Acad. Sci. USA*, **68**, 625–628.

Oesterhelt,D. (1972) *Hoppe-Seyler's Z. Physiol. Chem.*, **353**, 1554–1555.

Oesterhelt,D. and Stoeckenius,W. (1970) *Nature New Biol.*, **223**, 149–152.

Okamura,M.Y., Feher,G. and Nelson,W. (1982) In Govindjee (ed.), *Photosynthesis: Energy Conversion by Plants and Bacteria* Academic Press, New York, Vol. 1, pp. 195–272.

Omata,T., Murata,M. and Satoh,K. (1984) *Biochim. Biophys. Acta*, **765**, 403–405.

Parson,W.W. (1987) In Amesz,J. (ed.), *New Comprehensive Biochemistry: Photosynthesis*. Elsevier, Amsterdam, pp. 43–61.

Parson,W.W. and Ke,B. (1982) In Govindjee (ed.), *Photosynthesis: Energy Conversion by Plants and Bacteria*. Academic Press, New York, Vol. 1, pp. 331–384.

Pfister,K., Steinback,K.E., Gardner,G. and Arntzen,C.J. (1981) *Proc. Natl. Acad. Sci. USA*, **78**, 981–985.

Pugsley,A.P., Chapon,C. and Schwartz,M. (1986) *J. Biol. Chem.*, **256**, 2194–2198.

Rasmussen,O.F., Bookjans,G., Stummann,B.M. and Henningen,K.W. (1984) *Plant Mol. Biol.*, **3**, 191–199.

Rochaix,J.D., Dron,M., Rahire,M. and Maloe,P. (1984) *Plant Mol. Biol.*, **3**, 363–370.

Rossmann,M.G. (1979) *J. Appl. Crystallogr.*, **12**, 225–238.

Schmid,M.F., Weaver,L.H., Holmes,M.A., Gruetter,M.G., Ohlendorf,D.H., Reynolds,R.A., Remington,S.J. and Matthews,B.W. (1981) *Acta Crystallogr., A*, **37**, 701–710.

Schwager,P., Bartels,K. and Jones,A. (1975) *J. Appl. Crystallogr.*, **8**, 275–280.

Shuvalov,V.H. and Klimov,U.V. (1976) *Biochim. Biophys. Acta*, **440**, 587–599.

Sinning,I. and Michel,H. (1987a) In Biggins,J. (ed.), *Progress in Photosynthesis Research*. Martinus Nijhoff, Dordrecht, Vol. 3, pp. III.11.771–III.11.773.

Sinning,I. and Michel,H. (1987b) *Z. Naturforsch.*, **42**, Ser. C, 751–754.

Tiede,D.M., Prince,R.C., Reed,G.H. and Dutton,P.L. (1976) *FEBS Lett.*, **65**, 301–304.

Tronrud,D.E., Ten Eyck,L.F. and Matthews,B.W. (1987) *Acta Crystallogr., A*, **43**, 489–501.

Varghese,J.N., Laver,W.G. and Colman,P.M. (1983) *Nature*, **303**, 35–40.

Vermaas,W.F., Rutherford,A.W. and Hansson,Ö. (1988) *Proc. Natl. Acad. Sci. USA*, **85**, 8477–8481.

Wang,B.C. (1985) *Methods Enzymol.*, **115**, 90–112.

Weyer,K.A., Schäfter,W., Lottspeich,F. and Michel,H. (1987a) *Biochemistry (Wash.)*, **26**, 2909–2914.

Weyer,K.A., Schäfer,W., Lottspeich,F. and Michel,H. (1987b) In Papa,S., Chance,B. and Ernster,L. (eds), *Cytochrome Systems*. Plenum Publishing

Corporation, pp. 325–331.
Weyer,K.A., Lottspeich,F., Gruenberg,H., Lang,F., Oesterhelt,D. and Michel,H. (1987c) *EMBO J.*, **6**, 2197–2202.
Williams,J.C., Steiner,L.A., Ogden,R.C., Simon,M.I. and Feher,G. (1983) *Proc. Natl. Acad. Sci. USA*, **80**, 6505–6509.
Williams,J.C., Steiner,L.A., Feher,G. and Simon,M.I. (1984) *Proc. Natl. Acad. Sci. USA*, **81**, 7303–7307.
Williams,J.C., Steiner,L.A. and Feher,G. (1986) *Proteins: Structure, Function and Genetics*, **1**, 312–325.
Wilson,I.A., Skehel,J.J. and Wiley,D.C. (1981) *Nature*, **289**, 366–373.
Youvan,D.C., Bylina,E.J., Alberti,M., Requsch,H. and Hearst,J.E. (1984) *Cell*, **37**, 949–957.
Yu,F., Inouye,S. and Inouye,M. (1986) *J. Biol. Chem.*, **261**, 2284–2288.
Zinth,W., Kaiser,W. and Michel,H. (1983) *Biochim. Biophys. Acta*, **723**, 128–131.
Zinth,W., Knapp,E.W., Fischer,S.F., Kaiser,W., Deisenhofer,J. and Michel,H. (1985) *Chem. Phys. Lett.*, **119**, 1–4.
Zulauf,M., Weckstrom,K., Hayter,J.B., Degeorgio,V. and Corti,M. (1985) *J. Phys. Chem.*, **89**, 3411–3417.
Zurawski,G., Bohnert,H.J., Whitfeld,P.R. and Bottomley,W. (1982) *Proc. Natl. Acad. Sci. USA*, **79**, 7699–7703.